



HAL
open science

Impact of biogenic exudates on the dissolution and browning of stained glass windows

Valentina Valbi, Anne Perez, Aurélie Verney-Carron, Chloé Boutillez, Chloé Ranchoux, Chloé Fourdrin, Stéphanie Rossano

► To cite this version:

Valentina Valbi, Anne Perez, Aurélie Verney-Carron, Chloé Boutillez, Chloé Ranchoux, et al.. Impact of biogenic exudates on the dissolution and browning of stained glass windows. *International Biodegradation and Biodegradation*, 2022, 173, pp.105442. 10.1016/j.ibiod.2022.105442 . hal-03764535

HAL Id: hal-03764535

<https://hal.science/hal-03764535>

Submitted on 10 Nov 2022

HAL is a multi-disciplinary open access archive for the deposit and dissemination of scientific research documents, whether they are published or not. The documents may come from teaching and research institutions in France or abroad, or from public or private research centers.

L'archive ouverte pluridisciplinaire **HAL**, est destinée au dépôt et à la diffusion de documents scientifiques de niveau recherche, publiés ou non, émanant des établissements d'enseignement et de recherche français ou étrangers, des laboratoires publics ou privés.

1 ***Impact of biogenic exudates on the dissolution and browning of stained-glass windows***

2
3 Valentina Valbi ^a, Anne Perez ^a, Aurélie Verney-Carron ^b, Chloé Boutillez ^a, Chloé
4 Ranchoux^a, Chloé Fourdrin ^a, Stéphanie Rossano ^a.

5
6 ^a*Laboratoire Géomatériaux et Environnement, Univ Gustave Eiffel, F-77454 Marne-la-*
7 *Vallée, France*

8 ^b*Laboratoire Interuniversitaire des Systèmes Atmosphériques (LISA), UMR-CNRS 7583,*
9 *Université Paris Est Créteil, France*

10
11 **Abstract**

12 The browning phenomenon is a pathology affecting Mn-bearing medieval stained-glass-
13 windows in potash-lime-silicate glass system. In order to unravel the potential implication of
14 microorganisms in the appearance of this pathology, three model glasses respectively
15 containing no MnO, 1wt% and 2wt% MnO were altered at circumneutral pH, with and without
16 organic exudates (oxalic acid (OA) 1000 μM and siderophore desferrioxamine B (DFOB) 50-
17 1000 μM) likely to be produced by bacteria and fungi. In the absence of exudates, the
18 dissolution rates are inversely dependent on the Mn content of the glasses (0.8, 0.5 and 0.4 g
19 m⁻²d⁻¹ respectively for no MnO, 1wt% and 2wt% MnO glasses). In contact with exudates, an
20 opposite trend is observed. The prevalent mechanisms are interpreted as a strong ligand-
21 promoted dissolution for DFOB (dissolution rate increase up to 270%) and a dominant proton-
22 promoted dissolution for OA (dissolution rate increase up to 60%). When DFOB and OA are
23 added together, the effect of DFOB on the dissolution rate is prevailing, while OA effect is
24 tangible on the stoichiometry of the dissolution of the alteration. These results suggest that an
25 indirect biological activity could be involved in the mobilization of Mn from a Mn-bearing
26 glass, thus playing a role in the appearance of the browning phenomenon.

27
28 **Keywords**

29 Glass, dissolution, bioalteration, manganese, siderophore, oxalic acid
30
31

This article has been accepted for publication and undergone full peer review but has not been through the copyediting, typesetting, pagination and proofreading process, which may lead to differences between this version and the Version of Record. Please cite this article as:

<https://doi.org/10.1016/j.ibiod.2022.105442>

This article is protected by copyright. All rights reserved.

32 1. INTRODUCTION

33 Stained glass windows are enduring weathering for centuries in the atmosphere, being subject
34 to episodes of rain and high humidity that lead to the development of an alteration layer and to
35 the formation of secondary phases (Sterpenich and Libourel, 2001; Lombardo et al., 2013;
36 Gentaz et al., 2016). If the durability of glass strongly depends on its composition, the
37 mechanisms underlying glass alteration are mainly the same for all kind of silicate glasses. Two
38 main processes occurring simultaneously are described in literature: i) interdiffusion, that
39 involves ion exchange between modifier ions (mainly alkalis) and hydrogenated species (H^+ ,
40 H_3O^+ , H_2O) present in the environment and ii) hydrolysis of the silicate network iono-covalent
41 bonds ($Si-O-Si$ or $Si-O-Al$). The alteration kinetics and the relative contribution of each
42 mechanism depend on the glass composition, on the hygroscopic conditions (aqueous or
43 unsaturated medium) and on the experimental conditions such as pH, temperature and
44 saturation with respect to Si or other elements in solution (Gislason and Oelkers, 2003;
45 Cailleteau et al., 2008; Tournié et al., 2008; Gin et al., 2016; Verney-Carron et al., 2017). These
46 mechanisms lead to the formation of an altered layer that is alkali-depleted, hydrated and porous
47 and whose formation mechanisms are still discussed (e.g. Lenting et al., 2018 for more details).
48 For medieval stained glass windows, alteration experiments performed in solution have
49 highlighted the strong role of the interdiffusion process and hydrolysis / condensation reactions
50 in the formation of the alteration layer (Verney-Carron et al., 2017) and have allowed the
51 determination of kinetic laws (Sessegolo et al., 2017; Sessegolo et al., 2018; Sessegolo et al.,
52 2020).

53 Manganese can be present at concentration around 1-2 MnO wt% in archaeological glass and
54 stained-glass windows since it was used as a chromophore to obtain as less coloured as possible
55 glass (manganese was also called the glassmakers' soap) or purple shades (Mirti et al., 2002;
56 Quartieri et al., 2002; Jackson, 2005; Gulmini et al., 2009; Arletti et al., 2010; Gliozzo, 2017).
57 Manganese is also found at lower concentrations (0.2-0.5 MnO wt%) in natural basaltic glass
58 and other artificial glasses like nuclear waste glass (Staudigel and Hart, 1983; Thorseth et al.,
59 2003; Neaman et al., 2005; Chalmin et al., 2009; Gin et al., 2016) .

60 For Mn-bearing stained glass, a specific alteration pattern is observed. The browning
61 phenomenon is a pathology widely-spread in medieval stained glass windows of northern
62 Europe and characterized by Mn-rich brown spots (up to 7 MnO wt%) appearing at the surface

This article has been accepted for publication and undergone full peer review but has not been through
the copyediting, typesetting, pagination and proofreading process, which may lead to differences
between this version and the Version of Record. Please cite this article as:

<https://doi.org/10.1016/j.ibiod.2022.105442>

This article is protected by copyright. All rights reserved.

63 and subsurface of the glass altered layer (Bourleuf et al., 2011; Cagno et al., 2011; Schalm et
64 al., 2011; Ferrand et al., 2015; Nuyts et al., 2015). Those brown phases are small (ranging from
65 less than 10 μm to more than 100 μm), amorphous or poorly crystalline and they present a Mn
66 redox state between III and IV (Ferrand et al., 2015; Nuyts et al., 2015).

67 The mechanisms leading to the browning phenomenon are not yet understood. The manganese
68 contained in the glass might undergo a migration to the surface followed by an oxidation and /
69 or a precipitation within the altered layer in relation with biological activity (Perezy Jorba et
70 al., 1980; Drewello and Weissmann, 1997; Oriol et al., 2007). This is supported by previous
71 studies (Marvasi et al., 2009; Rölleke et al., 1999; Schabereiter-Gurtner et al., 2001; Carmona
72 et al., 2006; Piñar et al., 2013) that have identified numerous species of fungi and bacteria on
73 stained glass windows, attesting to the presence of a developed microbiome. If some studies
74 have been dedicated to the bioalteration of glass (Drewello and Weissmann, 1997; Gorbushina
75 and Palinska, 1999; Carmona et al., 2006; Rodrigues et al., 2014; Weaver et al., 2021), none of
76 them has investigated the microbiological mechanisms eventually leading to the browning.

77 In the environment, numerous bacteria, fungi, lichens and plants produce chelating molecules
78 such as low molecular weight organic acids and siderophores, which can strongly affect
79 minerals weathering by increasing the solubility and mobility of elements (Gadd, 1999;
80 Renshaw et al., 2002; Kraemer, 2004). The most common low molecular weight organic acids
81 produced by microorganisms are oxalic acid, citric acid, and acetic acid (Gadd, 1999; Neaman
82 et al., 2005; Calvaruso et al., 2013) and their effect on minerals dissolution has been
83 investigated (Bennett et al., 1988; Gadd, 1999; Cama and Ganor, 2006; Lazo et al., 2017; Li et
84 al., 2019). Siderophores have been studied and named after their ability to chelate iron, but
85 several studies demonstrated that they can also complex other metal cations such as Co, Mn,
86 Zn, Cu (Faulkner et al., 1994; Hernlem et al., 1994; Parker et al., 2004; Ahmed and Holmström.
87 2014; Schijf et al., 2015).

88 The dissolution of mineral/glass in aqueous media containing chelating ligands can be
89 decomposed in two distinct reactions. The proton-promoted dissolution is caused by the release
90 of metal ions from mineral/glass surface by proton exchange. The ligand-promoted dissolution
91 is caused by the complexation of metal ions from mineral/glass surface by organic molecules
92 with chelating properties (Furrer and Werner, 1986; Duckworth and Sposito, 2005b).

This article has been accepted for publication and undergone full peer review but has not been through
the copyediting, typesetting, pagination and proofreading process, which may lead to differences
between this version and the Version of Record. Please cite this article as:

<https://doi.org/10.1016/j.ibiod.2022.105442>

This article is protected by copyright. All rights reserved.

93 The dissolution mechanisms of Mn-bearing minerals were investigated in abiotic (Jun and
94 Martin. 2003; Luo et al., 2018) and biotic conditions (Tang et al., 2013; Li et al., 2019) as well
95 as in the presence of siderophores and small organic acids (Duckworth and Sposito, 2005a;
96 Peña et al., 2007; Akafia et al., 2014; Fischer et al., 2018, Saal and Duckworth 2010). Several
97 studies focused on DFOB-promoted dissolution of Fe and Mn-bearing minerals: hematite
98 (Hersman et al., 1995), goethite (Cheah et al., 2003), manganite (Duckworth and Sposito,
99 2005a), haussmanite (Peña et al., 2007), birnessite (Fischer et al., 2018), Fe, Co, Mn
100 oxyhydroxides (Akafia et al., 2014) and olivine (Torres et al., 2019). A few studies also
101 investigated the synergistic effect of siderophores with oxalate (Akafia et al., 2014; Saal and
102 Duckworth 2010).

103 Only few studies investigated the effect of siderophores on glass dissolution. Perez et al., 2015
104 and Perez et al., 2016 showed that siderophores can increase the dissolution rate of basaltic
105 glass because of their Fe-chelating properties.

106 In this work, the effect of a low molecular weight organic acid (LMWOA), oxalic acid (OA),
107 and of a siderophore, desferrioxamine B (DFOB), on the dissolution of a Mn-bearing potash-
108 lime silica glass is investigated. These two exudates were chosen because they are considered
109 as model molecules for LMOA (for OA) and hydroxamate siderophores (for DFOB). Oxalic
110 acid presents two carboxylic functional groups that are able to complex metallic cations,
111 moreover OA is commonly produced by many bacteria and fungi, thus making it a common
112 choice as a model LMOA for its ubiquity in the environment. DFOB is a linear siderophore
113 with strong chelating properties, it has three hydroxamate moieties and a terminal amine group,
114 it is commonly chosen as a model siderophore in dissolution studies because of its commercial
115 availability, making it a reference siderophore (Cheah et al., 2003; Kraemer, 2004; Duckworth
116 and Sposito, 2005b; Duckworth and Sposito, 2005a; Peña et al., 2007; Akafia et al., 2014; Schijf
117 et al., 2015; Fischer et al., 2018). The main objective is to quantify and compare the initial
118 dissolution rates for the glass compositions (with or without manganese) in different
119 experimental conditions involving these two biogenic exudates in one-ligand systems and two-
120 ligands systems. The possible mechanisms involved in glass dissolution in the presence of OA
121 and DFOB, and in their absence, are discussed.

122

123

This article has been accepted for publication and undergone full peer review but has not been through
the copyediting, typesetting, pagination and proofreading process, which may lead to differences
between this version and the Version of Record. Please cite this article as:

<https://doi.org/10.1016/j.ibiod.2022.105442>

This article is protected by copyright. All rights reserved.

124 **2. MATERIALS AND METHODS**

125 **2.1 Glass synthesis and characterization**

126 The potash-lime-silica composition of the studied glasses (Table 1) was chosen on the basis of
127 a typical composition of medieval stained-glass windows (Ferrand et al., 2015; Gentaz et al.,
128 2016; Sessegolo et al., 2018). Three compositions have been studied: a Mn-bearing glass (called
129 VM in the following text), a Mn-free glass (called VNM in the following text) and a glass
130 containing half the amount of Mn contained in VM (called VM1/2 in the following text).

131 Although present in most medieval compositions, Fe was not introduced in the glass
132 composition in order to target Mn behavior in the interaction of the glass with the exudates. Mn
133 and Fe might indeed be involved, and sometimes in concurrent ways, in similar chemical of
134 biochemical mechanisms (Duckworth et al, 2009).

135 Samples were prepared from ultrapure powdered oxides and carbonates (Alfa Aesar, Sigma-
136 Aldrich) that were previously dried in a furnace overnight (SiO₂, Al₂O₃, CaCO₃, MgCO₃,
137 NaCO₃, MnCO₃, K₂CO₃, KH₂PO₄), weighted and grounded in an agate mortar, then placed in
138 a Pt-Au crucible. The crucible was placed in a furnace Carbolite HTF 1700. The heating
139 program consisted of a temperature ramp to 600°C followed by a one-hour step at 600°C to
140 start decarbonation. Temperature was raised again to 1500°C. This temperature was held during
141 2 hours in order to homogenize the mixture. The melt was then quenched, crushed again, re-
142 melted and re-quenched to increase homogeneity. An annealing step at 530°C was applied for
143 two hours in order to eliminate the mechanical stresses present in the glass.

144 The composition of the obtained glass was checked by microprobe analysis on a Cameca SX
145 Five instrument. Samples were embedded in resin, polished and carbon-coated. A tension of 15
146 kV was used for the analysis, with a current of 4 nA. Silicate minerals were used as calibration
147 standards. Results of the measurements are reported in Table 1.

148 The glass was then grounded and sieved in order to collect the 100-200 µm powder size
149 fractions. This powder fraction was cleaned by sedimentation in acetone to remove residual fine
150 particles. The homogeneous size distribution was checked with a table scanning electron
151 microscopy equipped with an Energy Dispersive X-rays detector (SEM-EDX) TM3030. The
152 pristine glass powders were observed in environmental conditions of low vacuum with neither
153 sample preparation nor coating and backscattered electrons images were obtained at 15 kV.

154 BET measurements were performed by krypton adsorption in order to estimate the specific
This article has been accepted for publication and undergone full peer review but has not been through
the copyediting, typesetting, pagination and proofreading process, which may lead to differences
between this version and the Version of Record. Please cite this article as:

<https://doi.org/10.1016/j.ibiod.2022.105442>

This article is protected by copyright. All rights reserved.

155 surface area of the samples. Different batches of powder were prepared following the same
156 procedure and the average reactive surface area is $0.028 \pm 0.002 \text{ m}^2/\text{g}$. The Mn bearing glasses
157 both show a purple coloration due to the presence of Mn^{3+} ions. However, based on literature
158 results, these glasses probably contain a majority of Mn(II) (Nelson and White, 1980), thus a
159 mixture of Mn(II) and Mn(III) is more likely.

160

161 **2.2 Dissolution experiments**

162 First of all, the dissolution of the three glasses was studied in the absence of exudates. In order
163 to compare the initial dissolution rate, conditions far from equilibrium were chosen through a
164 low S/V ratio (surface area of glass / volume of solution). Batch experiments were conducted
165 in 240 ml PFA Savillex reactors. The reactors were previously cleaned in a nitric acid bath and
166 washed three times with Ultrapurewater (18.2 M Ω) (UPW) to reduce environmental pollutions.
167 The altering solutions were prepared with UPW buffered with NaHCO_3 1 mM in order to
168 stabilize the pH evolution during the dissolution experiment, in an effort to obtain comparable
169 experiments in terms of pH evolution for all the conditions tested. Carbonate buffer was chosen
170 to keep the system as simple as possible, as it has been proven that more complex buffers can
171 complex metal ions and so interfere with the dissolution mechanisms (e.g. Ferreira et al., 2015;
172 Tournié et al., 2013). The pH of the initial solution was adjusted with diluted HNO_3 to a starting
173 pH of 6.8 ± 0.1 . This solution (UPW with carbonate buffer at 6.8 pH) represents the control
174 conditions.

175 The dissolution behavior of VM and VNM was also investigated in the presence of the exudates.
176 Oxalic acid and/or DFOB were added to the control solution to obtain the final altering
177 conditions. The altering solutions can then be divided in two categories (one or two-ligands
178 systems). The one-ligand systems correspond to a series of dissolution experiments in several
179 aqueous solutions containing 1 mM Oxalic Acid (AlfaAesar) or Desferrioxamine B (mesylate
180 salt. Alfa Aesar) at concentrations of 50 μM , 100 μM , 250 μM , 500 μM and 1000 μM . The
181 two-ligand system consists in a series of dissolution experiments in different aqueous solutions
182 containing 1 mM OA and DFOB at concentrations ranging from 50 to 500 μM . The VNM glass
183 was submitted to the control condition, the one-ligand solution containing OA 1 mM and the
184 one-ligand solution containing DFOB 500 μM . Experimental conditions are listed in Table 2.

This article has been accepted for publication and undergone full peer review but has not been through the copyediting, typesetting, pagination and proofreading process, which may lead to differences between this version and the Version of Record. Please cite this article as:

<https://doi.org/10.1016/j.ibiod.2022.105442>

This article is protected by copyright. All rights reserved.

185 A blank sample was systematically collected before the introduction of the glass. After the
186 blank sampling, 100 mg of glass powder (with a size distribution between 100-200 μm) were
187 immersed in 200 ml of solution ($S/V = 0.14 \pm 0.01 \text{ cm}^{-1}$). The suspensions were continuously
188 shaken at 160 rpm at a controlled temperature of 25°C. Solution samples were collected during
189 the dissolution experiment at time 0, 3, 6 hours, 1, 2, 3 days. Each sampling was performed by
190 removing 3 ml aliquots using a 5 ml syringe and filtered with 0.45 μm cellulose-acetate syringe
191 filters. The total amount of sampled solution corresponds to less than 10% of the total starting
192 volume, to ensure a quasi-constant S/V. The pH was measured at every sampling with an
193 Ag/AgCl type electrode. Prior to ICP-OES analysis, collected samples and the calibrating
194 solutions were acidified to 5% with HNO_3 . The leachates were analyzed with a Perkin Elmer
195 Optima 8300 ICP-OES in order to determine the concentrations of dissolved Si, Al, Mg, Ca,
196 Mn, K. ICP calibration solutions were prepared by dissolving a commercial silicon standard
197 solution and a commercial multielement solution (Merck Chemicals) in UPW. Analytical
198 absolute errors on elemental concentrations were determined for each element by analyzing
199 several times the calibrating solutions. The analytical errors were calculated for each range of
200 concentration for each element by evaluating the accuracy of the measurement over the average
201 of 10 measurements. The percentage error is generally between 1 and 10% for all elements in
202 all concentration ranges evaluated, except for Si and K concentrations lower than 100 ppb
203 where the error is 10 to 50%.

204 The concentration values, after blank subtraction, were transformed in normalized mass loss
205 $NL_{(i)}$ (Equation 1) for each element i of each leachate sample in order to normalize the results
206 to the percentage of the concerned element within the glass composition and to the S/V ratio.

207

$$208 \quad NL_{(i)} = \frac{c_i - c_{i0}}{S/V \times x_i} \quad (1)$$

209

210 C_i is the concentration of the element i in solution, C_{i0} is the concentration of the element i in
211 the blank sample. S is the surface of glass exposed to the solution and V is the volume of the
212 solution. x_i is the mass fraction of the element i in the glass.

213 Initial rate of dissolution r_i (equation 2) was determined by plotting the $NL_{(i)}$ versus time and
214 adjusting a linear regression on the initial slope of the curve. Generally, 4 to 6 points were

This article has been accepted for publication and undergone full peer review but has not been through the copyediting, typesetting, pagination and proofreading process, which may lead to differences between this version and the Version of Record. Please cite this article as:

<https://doi.org/10.1016/j.ibiod.2022.105442>

This article is protected by copyright. All rights reserved.

215 chosen by picking the maximum number of linear points for each fit in order to obtain R^2 values
216 ≥ 0.99 for all fits.

217

$$218 \quad r_{(i)} = \frac{dNL_{(i)}}{dt} \quad (2)$$

219

220 The absolute error on the $NL_{(i)}$ was calculated using the propagation of uncertainty law, taking
221 into account the analytical ICP-OES error (10%), the uncertainty on the measure of reactive
222 surface area (8%), and the experimental error \pm SD for the two experimental replicates varying
223 for each point, while the error on V and x_i are estimated to be negligible. This absolute error
224 will be taken into account for the calculation of the uncertainties on the glass dissolution rate
225 for comparison with literature results. However, the uncertainty on the reactive surface area
226 affects in the same way all the elements and for sake of clarity it will not be taken into account
227 when showing the $NL_{(i)}$ results, that are meant to compare the behavior of the different elements
228 of the glass.

229 The leachates containing DFOB were also analyzed in a UV-1800 Shimadzu UV-VIS
230 spectrophotometer at the absorption wavelength of the Mn(III)HDFOB⁺ complex (310 nm)
231 determined by different authors in the literature (Faulkner et al., 1994; Duckworth and Sposito,
232 2005b). Absorbance intensities were plotted versus time in order to follow the formation of the
233 complex during the dissolution experiment. A schematic draw of the experimental design is
234 available in Figure 1.

235 To observe possible secondary phases linked to alteration, the altered glass powders were
236 embedded in epoxy resin, polished using SiC abrasive grinding papers and diamond polishing
237 suspensions, then carbon-coated and observed by SEM-EDX.

238 All the experiments conducted on VM and VNM glasses were repeated twice, except for the
239 control conditions that were repeated three times. The experiment in control conditions for
240 VM1/2 was only conducted once.

241

242

243

244

245

This article has been accepted for publication and undergone full peer review but has not been through the copyediting, typesetting, pagination and proofreading process, which may lead to differences between this version and the Version of Record. Please cite this article as:

<https://doi.org/10.1016/j.ibiod.2022.105442>

This article is protected by copyright. All rights reserved.

246 **3. RESULTS**

247 **3.1 pH and elemental concentrations**

248 The final pHs of all altering solutions are given in Table 2. As 1 mM NaHCO₃ is a mild buffer
249 (starting pH of 6.8±0.1), the pH of the altering solutions raised to higher values during the
250 experiments. This phenomenon is commonly observed in glass dissolution experiments due to
251 the interdiffusion mechanism leading to exchange of the alkali ions from the glass with
252 hydrogenated species (H⁺, H₃O⁺) from the solution (Cailleteau et al., 2008; Sessegolo et al.,
253 2020), leaving the solution impoverished in H⁺. Whatever the conditions, the pH trend was
254 similar with an average final pH between 8.3 and 9.3 (Table 2). For the control conditions,
255 small differences are observed for the three glasses, the altering solution has a final pH of
256 9.1±0.3 for VNM, 8.7 for VM1/2 and 8.5±0.3 for VM. The more Mn in the glass, the lower the
257 final pH. For the altering solutions containing the exudates, slightly higher final pH values are
258 observed for OA experiments (8.9 or 9.3) while DFOB experiments are characterized by lower
259 final pH values (8.3-8.9).

260 The concentrations of the elements released in the solution for each experimental condition of
261 the dissolution experiments have been measured by ICP-OES. For all the elements and in each
262 experimental system, the concentrations generally increase with time with small variations from
263 one replicate to another. Si concentrations increase until 2.5 - 15 ppm depending on the altering
264 conditions at the end of the experiment. As the solubility of amorphous silica, [Si], is around
265 54 ppm at T = 25°C and pH < 10, the experiments are as expected performed far from saturation
266 conditions.

267

268 **3.2 Normalized mass loss profiles and stoichiometry**

269 The average (for the three replicates) normalized mass losses (NLs) for Si, Al, Ca, Mg, Mn, K
270 are plotted as a function of time for the [Control] experiment in Figure 2 for the three glasses.
271 Due to the presence of Na in the buffer, this element is not displayed. P was not analysed. The
272 NL values indicate incongruent dissolutions. In control conditions for VNM glass, Ca, Mg and
273 K are preferentially released compared to Si (Figure 2a) while Al is less released than Si. In
274 VM1/2 and VM glasses, the same incongruent behaviour as in VNM glass dissolution is
275 observed, and Mn is released in a similar way as Si (Figure 2b-c). However, a significant
276 difference can be observed among the three glasses in the control conditions regarding the NL
This article has been accepted for publication and undergone full peer review but has not been through
the copyediting, typesetting, pagination and proofreading process, which may lead to differences
between this version and the Version of Record. Please cite this article as:

<https://doi.org/10.1016/j.ibiod.2022.105442>

This article is protected by copyright. All rights reserved.

277 values. The values of NL for VNM are higher at each sampling time (higher NL values around
278 2.3 g m^{-2}) than for the VM glass (higher NL values around 1.2 g m^{-2}), with an intermediate but
279 closer to VM behaviour of VM1/2 (higher NL values around 1.5 g m^{-2}).

280 For [OA 1 mM] experiments, both for VNM and VM, the NL values are generally slightly
281 higher than in the [Control] experiment and the stoichiometry of the dissolution is changed
282 (Figure 3a-b). K is preferentially released as compared to the alkaline earth elements, and there
283 is a drop in $\text{NL}_{(\text{Ca})}$ values between day 1 and day 2. Al is less released than Si, showing the
284 same behaviour as in control conditions. Mn also has the same behaviour as in control
285 conditions and is still released with Si. Significant differences can also be observed between
286 VNM and VM in OA conditions regarding the NL values. The values of NL are higher for
287 VNM at each sampling time (higher NL values around 3 g m^{-2}) than for VM glass (higher NL
288 values around 2.2 g m^{-2}).

289 In [DFOB 500 μM] experiments, for both glasses very high NL values are observed (higher NL
290 values $> 4 \text{ g m}^{-2}$), together with congruent dissolution behaviour, with a linear trend for all the
291 elements over the whole-time range (Figure 3c-d). Slight differences can be observed between
292 VNM and VM in DFOB conditions regarding the NL values. The values of NL are higher for
293 VM at each sampling time ((higher NL values around 5 g m^{-2}) than for VNM glass (higher NL
294 values around 4 g m^{-2}).

295 NL values for all the elements of VM glass in the two-ligand system [OA 1mM + DFOB 500
296 μM] are plotted on Figure 3e. $\text{NL}_{(\text{Si})}$ values are high (around 3.5 g/m^2 after 3 days) and similar
297 to those obtained in the corresponding DFOB one-ligand system. An incongruent dissolution
298 behaviour (preferential release of K and decrease of the Ca concentration after one day) is
299 observed, similar to the one observed in the OA one-ligand system. These effects can be
300 observed in the same manner for the whole range of DFOB concentrations used in the two-
301 ligand system (data not shown).

302 An enhancement of NL values related to the increasing concentration of DFOB in solution is
303 observed for all the elements of VM glass (shown for Mn as an example in Figure 4a). A strong
304 increase in the NL values is observed between the control [C] experiment and the lowest
305 concentration of DFOB (50 μM) but it is not linear with DFOB concentration. This has been
306 observed in the one-ligand system as well as in the two-ligands system.

307

This article has been accepted for publication and undergone full peer review but has not been through
the copyediting, typesetting, pagination and proofreading process, which may lead to differences
between this version and the Version of Record. Please cite this article as:

<https://doi.org/10.1016/j.ibiod.2022.105442>

This article is protected by copyright. All rights reserved.

308 **3.3 UV-VIS absorbance**

309 UV-VIS measurements of the absorption of the Mn(III)HDFOB⁺ complex at 310 nm are plotted
310 in Figure 4b. The absorbance of the complex increases with the alteration time and as a function
311 of DFOB concentration, indicating an increase in Mn concentration in solution in good
312 agreement with NL results. The effect of the DFOB concentration is again reported as being
313 non-linear.

314 The concentration of the complex Mn(III)-HDFOB⁺ has been evaluated using UV-VIS spectra
315 and considering a molar extinction coefficient ϵ equal to 2060 M⁻¹ cm⁻¹ (Duckworth and
316 Sposito, 2005b; Duckworth and Sposito, 2005a). The obtained concentration values (Table S1
317 supplementary materials) are of the same order of magnitude and comparable within
318 experimental error to the concentrations of Mn obtained from the alteration solution by ICP-
319 OES.

320

321 **3.4 Initial dissolution rates**

322 The Si initial dissolution rates (r_i), commonly used in glass dissolution experiments as an
323 indicator of dissolution, are useful to compare different altering conditions. In this work, they
324 were calculated for all the glasses for each dissolution condition tested. All “dissolution rates”
325 mentioned in the following text will always refer to Si initial dissolution rates reported in Table
326 2.

327 In the control conditions, VNM glass is characterized by a higher dissolution rate (0.80 g m⁻²
328 d⁻¹) than VM (0.40 g m⁻² d⁻¹) and VM1/2 glass (0,50 g m⁻² d⁻¹). [OA 1 mM] enhances the
329 dissolution rate for both VNM (x1.4) and VM (x1.6) glasses. [DFOB 500 μ M] also enhances
330 the dissolution rate for both VNM (x1.7) and VM (x3.6) glasses.

331 The dissolution rate for VM glass is strongly enhanced even for small concentrations of DFOB.
332 With 50 μ M of siderophore in solution, the dissolution rate is already doubled as compared to
333 the control experiment (from 0.40 to 0.83 g m⁻² d⁻¹). It keeps increasing with the increase of
334 DFOB molecules in solution. For [DFOB 1000 μ M], the initial dissolution rate is almost four
335 times higher than the r_{Si} in control conditions. As already observed on the NL values in Figure
336 4, the increase in dissolution rate in the presence of DFOB for Mn-bearing glass is however not
337 proportional to the DFOB concentration and this increase in rates is less and less important as
338 the DFOB concentration increases.

This article has been accepted for publication and undergone full peer review but has not been through
the copyediting, typesetting, pagination and proofreading process, which may lead to differences
between this version and the Version of Record. Please cite this article as:

<https://doi.org/10.1016/j.ibiod.2022.105442>

This article is protected by copyright. All rights reserved.

339 In the two-ligands system, a slight increase in the initial dissolution rate is observed when OA
340 is simultaneously present (in the order of x1.2) as compared to the DFOB one-ligand system
341 for the same DFOB concentrations, except for the [OA 1mM + 500 μ M DFOB] condition.

342

343 4. DISCUSSION

344 *4.1. The effect of the glass composition on the dissolution rate in control conditions*

345 The three glasses have very similar compositions except for the amount of Mn (Table 1), but in
346 the same control conditions they exhibit different dissolution rates (Figure 5). In order to assess
347 the effect of glass composition on the dissolution rate, several parameters can be considered.
348 The most immediate approach consists in investigating the differences in the dissolution
349 behavior among the glasses observed might be related to the Si content. Cailleteau et al., 2008b
350 showed that for three series of glasses (borosilicates, aluminosilicates and lead-silicates) the
351 dissolution rates strongly increase when lowering the silica content (SiO₂ content varying from
352 79 to 47 oxide wt%). In our study, the difference in silica content between VM and VNM (51.5
353 and 52.4 oxide wt%, respectively) is small (Table 1) and, if this difference could have a
354 significant effect on glass reactivity, VM should present a higher dissolution rate than VNM
355 (which is not the case, as showed in Table 2 and Figure 5). Besides, VNM has also a higher
356 K₂O content than VM (18.8 and 18.3 wt%, respectively), which should favor interdiffusion.
357 However, these small composition variations could both induce, if significant, opposite effects
358 on dissolution rates (Woisetschlager et al., 2000; Wolff-Boenisch et al., 2004; Melcher and
359 Schreiner, 2006; Cailleteau et al., 2008b; De Ferri et al., 2014). A more general and complex
360 compositional parameter is the Non-Bridging Oxygens over Tetrahedra ratio NBO/T (Jantzen
361 and Plodinec, 1984; Mysen and Richet, 2005; Trcera et al., 2011). Its calculation, assuming that
362 only Al and Si are former oxides in tetrahedral sites, gives very close values for the glasses of
363 this study (VNM: 1.68, VM1/2: 1.73, VM: 1.74) and a surprising trend as the most
364 depolymerized glasses display the lowest alteration rate (higher NBO/T values correspond to
365 less polymerized glasses). Moreover, the structural role of other intermediate elements such as
366 P and Mn is not known. In the extreme case where all Mn is considered as a network former,
367 the NBO/T of VM1/2 and VM is 1.64 and 1.55 respectively, which leads to an inverse trend.
368 The use of this parameter is thus very sensitive to small changes of composition and requires
369 detailed data on the structural role of each element. In any case, the results highlight that Mn
This article has been accepted for publication and undergone full peer review but has not been through
the copyediting, typesetting, pagination and proofreading process, which may lead to differences
between this version and the Version of Record. Please cite this article as:

<https://doi.org/10.1016/j.ibiod.2022.105442>

This article is protected by copyright. All rights reserved.

370 can have a significant role on the glass composition and structure and on its alteration as a low
371 percentage of MnO appears to have a significant effect in reducing the initial dissolution rate
372 of the glass in UPW. This behavior is concomitant with the pH evolution. The final pH values
373 gradually increase when the Mn content decreases (8.5 for VM, 8.7 for VM1/2 and 9.1 for
374 VNM). The pH difference among the three glasses after 3 days is also consistent with
375 dissolution rate results: the faster the dissolution, the higher is the rise in pH.

376 In consequence, the results suggest that the introduction of a low percentage of MnO oxide
377 wt%, which is the most significant difference between VM, VM1/2 and VNM (2 and 1 MnO
378 oxide wt% respectively for VM and VM1/2), is responsible for the change in the dissolution
379 behavior of the glass during the first stages of the alteration.

380 The Si dissolution rates obtained in the control conditions for both VM, VM1/2 and VNM
381 glasses can be compared to the values obtained by Sessegolo et al., 2020 on a similar potash-
382 lime silica glass containing both Mn and Fe. At 25°C and circumneutral pH, the dissolution rate
383 is 0.23 g m² d⁻¹, which is lower than for VM. This difference can be attributed to the presence
384 of Fe in the glass used by Sessegolo et al., 2020 glass, that could have a stabilizing effect on
385 the glass structure, similarly to Mn, as suggested by the comparison of VM with VM1/2 and
386 VNM glasses. In low SiO₂-content medieval-like potash-lime silicate glasses, a low percentage
387 of Fe or Mn has a significant impact on the durability of the glass during the first stages of the
388 alteration.

389

390 ***4.2 Glass alteration mechanisms with exudates***

391 ***4.2.1 One-ligand system: Oxalic acid***

392 An increase in dissolution rate is observed for VM in presence of [OA 1mM] compared to the
393 control conditions (Table 2) in good agreement with previous works on dissolution of silicate
394 minerals (Drever and Stillings, 1997; Gislason and Oelkers, 2003; Cama and Ganor, 2006).

395 The increase in dissolution rate in the presence of organic acids is generally attributed to two
396 possible mechanisms often occurring simultaneously: the proton-promoted dissolution where
397 the driving force is the ion-exchange between the protons in solutions and the cations in the
398 mineral, and the ligand-promoted dissolution where the driving force is the complexation of
399 elements from the substrate by a chelating functional group in the acid molecule (Cama and
400 Ganor, 2006; Salek et al., 2013).

This article has been accepted for publication and undergone full peer review but has not been through
the copyediting, typesetting, pagination and proofreading process, which may lead to differences
between this version and the Version of Record. Please cite this article as:

<https://doi.org/10.1016/j.ibiod.2022.105442>

This article is protected by copyright. All rights reserved.

401 In this work, the starting pH was of 6.8 and raised to higher values (8.5 - 9) with the same trend
402 for all the conditions. However, significant differences between final pH values were observed
403 for different ligand systems and can be used to better understand the dissolution mechanisms.
404 The increase of pH is observed whatever the ligand systems. However higher values (8.5 - 9)
405 are attained in the OA experiments. Moreover, a preferential release of K is observed in the
406 presence of OA (Figure 3a-b). This suggests that an ion-exchange promoted dissolution
407 mechanism is promoted in presence of OA.

408 Regarding the ligand-promoted dissolution, the complexation effect is assumed to be negligible
409 for soluble elements such as Na, K, Ca, Mg (Huang and Keller, 1972; Drever and Stillings,
410 1997; Poulson et al., 1997). Oxalate adsorption on quartz surfaces is also considered negligible
411 and no complexation of Si was observed (Huang and Keller, 1972; Fein and Hestrin, 1994;
412 Poulson et al., 1997), suggesting that oxalate has little or no effect on quartz, so Si complexation
413 by OA molecules is not taken into account in glass dissolution studies (Perez et al., 2015). The
414 increase in dissolution rates of silicate minerals by OA is generally linked to the extraction of
415 Al from the framework (in tetrahedral sites) that implements the breakdown of the silica
416 tetrahedra of the minerals and accelerates the dissolution of Si (Huang and Keller, 1972). A
417 similar effect could be present in glass dissolution and a ligand-promoted dissolution could be
418 at work through the complexation of Al.

419 Few studies investigated the dissolution of Mn-bearing minerals in the presence of organic
420 acids. Li and Schwartz, 2004; Wang and Stone, 2006 identified the complexation of Mn by OA
421 as one of the possible responsible mechanisms for the dissolution of MnO₂ and MnOOH.
422 Hausrath et al., 2009 found that during basaltic and granitic rocks dissolution, elements such as
423 Zr, Sc and Mn showed a strong enrichment in solution in the presence of citrate, suggesting a
424 correlation between the presence of these elements and the complexing properties of the citrate.
425 The comparison of the results for VM and VNM glasses in the presence of [OA 1 mM] shows
426 that the Mn-bearing VM glass undergoes a slightly stronger increase in dissolution rate in the
427 presence of OA (increase of ~60% going from 0.40 to 0.64 g m⁻² d⁻¹) than the Mn-free VNM
428 glass (increase of ~40% going from 0.80 to 1.13 g m⁻² d⁻¹) as plotted in Figure S2a in
429 supplementary materials. This different reactivity of the two glasses in the presence of OA and
430 the fact that the Mn-bearing glass is more affected by the presence of the ligand suggests a
431 specific interaction/complexation between OA and Mn. However, although a difference is

This article has been accepted for publication and undergone full peer review but has not been through
the copyediting, typesetting, pagination and proofreading process, which may lead to differences
between this version and the Version of Record. Please cite this article as:

<https://doi.org/10.1016/j.ibiod.2022.105442>

This article is protected by copyright. All rights reserved.

432 observed, the effect of OA on the dissolution rates of the two glasses is quite similar, meaning
433 that the complexation of Mn by OA is present, but weak.

434 Another effect observed in the presence of OA for both glasses is the drop of Ca in solution
435 after one day of experiment (Figure 3a-b). This was explained by the SEM-EDX observations
436 of Ca-rich crystals at the surface of the altered glass powders (Figure S1 supplementary
437 materials), attributed to the complexation and precipitation of calcium oxalate (Welch and
438 Ullman, 1993; Perez et al., 2015).

439 Wolff-Boenisch and Traina, 2007 stated that the precipitation of calcium oxalate would
440 decrease the efficiency of the ligand-promoted dissolution by lowering the number of free
441 molecules present in solution. Thus, it is necessary to take into account that the ligand-promoted
442 mechanism on Al and Mn could be limited by the release of Ca in solution. Overall, the results
443 on the dissolution of VM and VNM glasses in the presence of OA glass show that multiple
444 mechanisms operate jointly: the promotion of the ion-exchange between H^+ and K^+ , the
445 complexation of Al and Mn, and secondary phases precipitation.

446

447 **4.2.2 One-ligand system: DFOB siderophore**

448 A strong increase in dissolution rates for VM and VNM was observed in the presence of DFOB
449 when compared to the control conditions (Table 2).

450 Three mechanisms of dissolution are reported in the literature for Mn-bearing minerals in
451 presence of siderophores: the proton-promoted dissolution, the ligand-promoted dissolution and
452 the reductive-dissolution.

453 In this work, in the presence of DFOB, the pH raised from the initial 6.8 to a final average pH
454 of around 8.7. According to the literature, reductive dissolution and proton-promoted
455 dissolution are either small or negligible above pH 7, while ligand-promoted dissolution rates
456 are generally invariant with respect to changing pH (Cheah et al., 2003; Duckworth and Sposito,
457 2005a; Peña et al., 2007, Fischer et al., 2018). Thus, we will only discuss ligand-promoted
458 dissolution, that is prevalent in the pH range studied in this work.

459 We observed for both VNM and VM glasses (Table 2, Figure 3c-d) a strong effect of DFOB
460 both on kinetics (increase in dissolution rates) and stoichiometry (congruent dissolution). The
461 congruent dissolution is a sign of a destabilization of the silicate network leading to the release
462 of all the glass elements in solution, including the network formers. Si is the major network-

This article has been accepted for publication and undergone full peer review but has not been through the copyediting, typesetting, pagination and proofreading process, which may lead to differences between this version and the Version of Record. Please cite this article as:

<https://doi.org/10.1016/j.ibiod.2022.105442>

This article is protected by copyright. All rights reserved.

463 forming element in the glass structure and the rupture of the Si-O bonds is considered as the
464 rate-limiting step in dissolution (Oelkers and Gislason, 2003). As stated by Perez et al. (2015),
465 we can assume that the effect of Si complexation by both OA and DFOB on the dissolution of
466 glass is negligible. As a consequence, the increase in Si dissolution rates in the presence of
467 DFOB can be indirectly attributed to the complexation of metallic cations at the glass surface,
468 which causes a destabilization of the silica network, in favour of its global dissolution and leads
469 to a congruent behaviour.

470 Neaman et al., 2005 showed how Fe complexation in basaltic rocks can destabilize the silica
471 network, resulting in higher dissolution rates. The same effect was demonstrated on basaltic
472 glass by Perez et al., 2015 and Perez et al., 2016, who highlighted the importance of Fe³⁺ and
473 Al³⁺ complexation respectively in a Fe-bearing and in an Fe-free glass during glass dissolution
474 in the presence of siderophores. It is possible to draw a parallel between the study of Perez et
475 al., 2015 and Perez et al., 2016 and the effect of DFOB on glass dissolution by the complexation
476 of Al³⁺ in both VNM and VM glass. However, the complexation of Al³⁺ may not be the only
477 driving force for dissolution in the case of VM glass as the complexation of Mn was also
478 observed through detection of Mn-siderophore complex by UV-VIS measurements (Figure 4b).
479 Moreover, the comparison of the effect of DFOB 500 µM on VM and VNM shows that DFOB
480 has a stronger effect on VM glass with an increase in dissolution rate of ~250% (from 0.40 to
481 1.43 g m⁻² d⁻¹) while an increase of only ~60% was observed for VNM glass (from 0.80 to 1.32
482 g m⁻² d⁻¹) as plotted in Figure S2b in supplementary materials. Thus, if we attribute the increase
483 in dissolution rate of VNM to the complexation of Al we should assume that the same increase
484 is observed for VM dissolution in the presence of DFOB. However, the effect of Al
485 complexation on VM glass dissolution roughly accounts for 1/4 of the total increase in
486 dissolution rate for this glass. In consequence, another effect must be taken into account and
487 could be attributed to a strong Mn complexation.

488 The formation of the complex Mn(III)-HDFOB⁺ (stable at pH in the range of 7-11.3) was
489 confirmed for all the DFOB dissolution experiments by UV-VIS measurements at 310 nm
490 (Figure 4b). According to literature, there can be two main mechanisms of formation of the
491 complex Mn(III)HDFOB⁺: the direct formation by dissolution of Mn³⁺ mineral phases, or the
492 oxidation of an intermediate Mn(II)-DFOB complex (Duckworth and Sposito, 2005b;
493 Duckworth and Sposito, 2005a). The oxidation state of Mn in VM glass is not known, but as

This article has been accepted for publication and undergone full peer review but has not been through
the copyediting, typesetting, pagination and proofreading process, which may lead to differences
between this version and the Version of Record. Please cite this article as:

<https://doi.org/10.1016/j.ibiod.2022.105442>

This article is protected by copyright. All rights reserved.

494 stated before (section 2.1) the presence of a mixture of Mn^{2+} and Mn^{3+} is expected (Nelson and
495 White, 1980; Ferrand et al., 2015; Nuyts et al., 2015). In the dissolution experiments of VM
496 glass in the presence of DFOB, the Mn(III)HDFOB^+ complex could be formed via both
497 mechanisms: the Mn^{3+} present in the glass is leached and directly complexed to form
498 Mn(III)HDFOB^+ , while Mn^{2+} present in the glass is either oxidized in solution or forms a
499 Mn(II)-DFOB complex that immediately evolves to Mn(III)HDFOB^+ (Duckworth and Sposito,
500 2005a; Duckworth and Sposito, 2005b). The measured total dissolved Mn concentration did not
501 exceed the total siderophore concentration and the values of concentration of the complex
502 Mn(III)-HDFOB^+ are close within the experimental error to the concentration of Mn detected
503 in solution (Table S1 in supplementary materials). This suggests that all Mn present in solution
504 is complexed by the DFOB.

505 A small amount of siderophore (50 μM) is able to more than double the Si dissolution rate
506 calculated for the control conditions (Table 2) and an increase in dissolution was observed with
507 the increase in the siderophore concentrations from 50 to 500 mM (Figure 4a-b, Table 2).
508 However, the increase in dissolution rates is not proportional to the concentration of DFOB and
509 no concentration effect is no longer observed between 500 and 1000 μM . This result is not in
510 agreement with the work of Duckworth and Sposito, 2005a on haussmanite dissolution, in
511 which the dissolution rate was shown to be directly proportional to the surface concentration of
512 adsorbed DFOB and to vary as a function of DFOB concentration (Cheah et al., 2003;
513 Duckworth and Sposito, 2005a). MnO_2 representing only 2% of the total composition of the
514 VM glass, the observed “threshold effect” effect might be due to the saturation of the molecules
515 in solution with respect to the available sites at the surface of the glass. A rough calculation was
516 used to estimate the number of moles of Mn atoms available at the surface of the VM glass.
517 The surface Mn sites on the glass were estimated by taking into account the amount of Mn
518 moles in the glass (0.028) and the element ionic radius (1.4 Å) together with the data for all the
519 other elements in the glass, for an obtained value of ~1% of glass surface occupied by Mn
520 atoms. We know that the exposed glass surface in the dissolution experiments is of 0.0028 m^2
521 for 100 mg of glass, thus the Mn exposed surface can be estimated at roughly $2.3 \cdot 10^{-5} \text{m}^2$. These
522 data reported in terms of number of moles of Mn at the surface and compared to the number of
523 moles of DFOB in 200 ml of altering solution with the lowest concentration of siderophore used
524 in this study (50 μM) show that the amount of DFOB moles already exceeds the number of Mn

This article has been accepted for publication and undergone full peer review but has not been through
the copyediting, typesetting, pagination and proofreading process, which may lead to differences
between this version and the Version of Record. Please cite this article as:

<https://doi.org/10.1016/j.ibiod.2022.105442>

This article is protected by copyright. All rights reserved.

525 moles exposed to the solution by 10^4 . This gap between DFOB and Mn concentrations may
526 explain why the impact of DFOB on dissolution rates tends to decrease with increasing DFOB
527 concentrations. Fischer et al., 2018 also observed a threshold effect while studying the DFOB-
528 promoted dissolution of birnessite and suggest that once a DFOB concentration threshold is
529 reached, the number of active sites on the birnessite crystal surface limits the reaction rate.
530 The pathway by which siderophores remove metals from minerals has been widely investigated,
531 but many details of the process, in particular the effect on the crystal structure, remain unclear
532 (Fischer et al., 2018). The chemisorption of siderophores to metal centers at mineral surfaces
533 has been supported by many studies with many characterization techniques (Holmén and Casey,
534 1996; Kalinowski et al., 2000; Kendall and Hochella, 2003). Fischer et al., 2018 showed that
535 the occupancies of the Mn within the octahedral sheets of birnessite continuously decreased
536 during siderophore-promoted dissolution. As already said, for VM glass in the presence of
537 DFOB it is possible to attribute the strong increase in dissolution rates to the complexation of
538 both Al and Mn. This might be responsible for the weakening of the network structure and
539 consequently of the enhancement of the whole silicate network dissolution. In literature, the
540 dissolution rate enhancement of manganite is attributed to the polarization of Mn-O bonds in
541 the mineral structure and increase in the rate at which these bonds break (Duckworth and
542 Sposito, 2005a). The results suggest that, once the mobilization of Al and Mn is enhanced by
543 the presence of strong chelating molecules, the whole silicate network is destabilized.
544 This strong enhancement of dissolution rates is already obtained at weak concentrations of
545 DFOB. Low concentrations are closer to the real concentrations possibly found in the
546 environment (Cheah et al., 2003) and attest for the strong impact of those molecules on
547 biogeochemical cycles. Moreover, those molecules act catalytically because once the metal ion
548 is taken up by the organisms, the siderophore can restart the process, so that low concentrations
549 can be really effective (Hersman et al., 1995; Kalinowski et al., 2000).

550

551 ***4.2.3 One-ligand systems: Comparison between OA and DFOB***

552 In this work, it is also possible to compare the effect of different ligands at the same
553 concentration, [OA 1 mM] and [DFOB 1 mM] systems, on the dissolution of the VM glass. In
554 the presence of [OA 1 mM], an increase in the dissolution rate of ~60 % (from 0.40 to 0.64 g
555 $\text{m}^{-2} \text{d}^{-1}$) was observed compared to the control conditions (Table 2). For the same DFOB

This article has been accepted for publication and undergone full peer review but has not been through the copyediting, typesetting, pagination and proofreading process, which may lead to differences between this version and the Version of Record. Please cite this article as:

<https://doi.org/10.1016/j.ibiod.2022.105442>

This article is protected by copyright. All rights reserved.

556 concentration, the increase is of ~270% (from 0.40 to 1.50 g m⁻² d⁻¹). It thus appears that, for
557 the same concentration, OA has a smaller effect on the dissolution rate than DFOB, in
558 agreement with the corresponding lower values of the complex formation constant (Table S2
559 in supplementary materials). Organic ligands that have stronger equilibrium constants with the
560 elements of the mineral/glass substrate are more effective in enhancing dissolution rates, and
561 the greatest influence was observed with species displaying the greatest number of binding
562 sites. The enhancement of dissolution rates by the mechanism of ligand-promoted dissolution
563 is driven by the complexation of metallic cations in solution and at the surface of the substrate.
564 This means that a ligand that forms a stronger complex and which has then a higher equilibrium
565 constant is more effective in promoting the dissolution because i) it will remove metallic cations
566 from the substrate's surface more efficiently and ii) it will increase the apparent solubility of
567 the cation in solution, encouraging its dissolution. The correlation of the increase in dissolution
568 rate with the complex formation constant is verified when comparing the results observed in
569 the present and previous studies on glasses or minerals (Neaman et al., 2005; Hausrath et al.,
570 2009; Perez et al., 2015).

571 Previous studies stated that one molecule of DFOB is sufficient to complex trivalent cations,
572 while two or three OA molecules are required to simultaneously adsorb on two neighbouring
573 edge aluminol sites (Cama and Ganor, 2006) and form a highly stable complex (Kruft et al.,
574 2013; Wolff-Boenisch & Traina, 2007). Perez et al., 2015 concluded that for basaltic glass, OA
575 should be at least three times more concentrated than DFOB to promote the release of Fe³⁺ in
576 the same manner as DFOB does. However, a direct comparison of the complexing properties
577 of these two ligands is not possible because we showed that several coexistent mechanisms
578 occur during the dissolution in the presence of OA and it is hard to isolate the contribution of
579 the ligand-promoted one. In fact, in this study, low concentrations of DFOB were tested and
580 even the weakest DFOB concentration (50 µM), is more effective than [OA 1 mM] in enhancing
581 the glass dissolution (Table 2), even with a concentration of OA more than 10 times higher than
582 the siderophore concentration.

583

584 ***4.2.4 Two-ligands system: synergistic effect?***

585 In natural systems, the production of siderophore is often associated to the production of low
586 molecular weight organic acids, but only a few studies investigate the synergistic effect on

This article has been accepted for publication and undergone full peer review but has not been through
the copyediting, typesetting, pagination and proofreading process, which may lead to differences
between this version and the Version of Record. Please cite this article as:

<https://doi.org/10.1016/j.ibiod.2022.105442>

This article is protected by copyright. All rights reserved.

587 dissolution mechanisms of little organic molecules like oxalic acids with siderophores (Cheah
588 et al., 2003; Reichard et al., 2005; Akafia et al., 2014, Saal and Duckworth, 2010). This
589 synergistic effect can be observed through a dissolution rate in the two-ligands system that is
590 the sum of the dissolution rates in the two separate one-ligand systems and in some cases even
591 more than the sum of the two one-ligand rates (Akafia et al., 2014). This effect is attributed to
592 oxalate acting like a shuttle that delivers metallic ions to siderophores dissolved in solution
593 (Cheah et al., 2003; Akafia et al., 2014).

594 In the present work, the systems combining OA and DFOB are characterized by NL values that
595 are similar to the one-ligand DFOB system. The difference in dissolution rates between the two-
596 ligands system and the corresponding DFOB one-ligand system is not significant within the
597 experimental error for most of the conditions (Table 2, Figure 6).

598 The results suggest that the presence of DFOB mostly controls the kinetics by ligand-promoted
599 dissolution, while OA only increases the release of K by interdiffusion and causes the
600 precipitation of Ca-oxalates (Figure 3e). In the presence of DFOB, the (weak) complexing
601 effect of OA seems negligible compared to the stronger DFOB complex formation constants
602 with the glass elements. This result is in agreement with the work of Akafia et al., 2014, in
603 which the OA-DFOB synergistic effect was shown to be not that significant for MnOOH when
604 compared for example to FeOOH. However, a synergistic effect of OA and DFOB on the
605 dissolution of Mn-bearing minerals was observed by Saal and Duckworth, 2010. The
606 synergistic effect could therefore also be substrate-dependent and be less important for glasses
607 than for minerals.

608 The absence of a synergistic effect can also be attributed to a saturation effect linked to the
609 presence of too many molecules in solution. A marked threshold effect is observed after 250
610 μM (Figure 6), that confirms the existence of a saturation effect that inhibits the dissolution at
611 higher ligands concentrations. Neaman et al., 2005 already observed a slight decrease of
612 dissolution rates for basaltic glass at high organic acids concentration and Cheah et al., 2003
613 showed that goethite dissolution rates reach a plateau at OA concentrations above 5 mM and 1
614 mM for Wolff-Boenisch and Traina, 2006.

615
616
617

This article has been accepted for publication and undergone full peer review but has not been through the copyediting, typesetting, pagination and proofreading process, which may lead to differences between this version and the Version of Record. Please cite this article as:

<https://doi.org/10.1016/j.ibiod.2022.105442>

This article is protected by copyright. All rights reserved.

618 **4.3 The role of Mn in the glass**

619 The presence of Mn in glass has been shown to decrease the dissolution rate in control
620 conditions. Even if its structural role is not precisely known, the comparison between the
621 alteration of Mn-free (VNM) and Mn (VM) glasses can provide some elements of
622 consideration. Chemical elements that have an effect of decreasing the dissolution rate of a
623 glass are more likely to have a former or a stabilizing role in the glass structure (Woisetschläger
624 et al., 2000; Wolff-Boenisch et al., 2004; Melcher and Schreiner, 2006; Cailleteau et al., 2008b;
625 De Ferri et al., 2014). Moreover, the complexation of Mn by siderophores involves a significant
626 increase of the dissolution rate for VM, whereas it has a weaker effect for the VNM glass. This
627 could be a supplementary clue about the structural role of Mn that, when removed from the
628 glass, causes a deep destabilization of the glass structure and an increase in dissolution rate,
629 favoring the hypothesis of a stabilizing effect of this element on the structure of a potash-lime
630 silicate glass.

631 In conclusion, in presence of biogenic exudates, Mn seems to be strongly involved in ligand-
632 promoted dissolution mechanisms. As the key-role of Mn is probably related to its structural
633 role and oxidation state, future work will need to investigate the structural role of manganese
634 (Galoisy et al., 2001; Chalmin et al., 2009) in order to enlighten its role during the dissolution
635 experiments.

636

637 **4.4 Implications for the understanding of the browning phenomenon of stained-glass** 638 **windows.**

639 In the environment, most bacteria and fungi produce low molecular weight organic acids and
640 siderophores (Kraemer et al., 1999; Kalinowski et al., 2000; Neubauer et al., 2000; Renshaw et
641 al., 2002) with few exceptions. Thus, these kinds of exudates are also likely to be produced by
642 micro-organisms on stained-glass windows, or in the soil for archaeological glass. These
643 organic molecules typically exhibit lower ranges of concentration than those studied in the
644 present work. Oxalate is a simple carboxylic acid that is relatively abundant in soil and
645 groundwater, with concentrations up to 1 mM (Fox and Comerford, 1990; Cama and Ganor,
646 2006). In marine systems and groundwater, depending on authors, reported concentrations of
647 siderophores can vary between 0.3 and 7 nM (Kraemer, 2004) or are in the order of hundreds
648 of micromoles (Hersman et al., 1995). However, close to the interface between micro-

This article has been accepted for publication and undergone full peer review but has not been through the copyediting, typesetting, pagination and proofreading process, which may lead to differences between this version and the Version of Record. Please cite this article as:

<https://doi.org/10.1016/j.ibiod.2022.105442>

This article is protected by copyright. All rights reserved.

649 organisms and solid phases, the local concentrations of organic ligands and of siderophores can
650 locally increase by several orders of magnitudes (Ahmed and Holmström, 2014). For a bacterial
651 microniche, siderophore concentrations are indeed expected from 10 μM to few mM (Hersman
652 et al., 1995). This bacterial microniche can be compared to specific localized conditions on the
653 surface of stained glasses where a microfilm of water can be formed and lead to the formation
654 of advanced alteration features (Asay and Kim, 2005; Bernardi et al., 2006; Gentaz et al., 2011).
655 These conditions could favour the synthesis of siderophores and organic acids and their
656 interaction with stained-glass windows. It has been showed in this work that the presence of
657 these molecules can lead to an increased solubilization of the elements of the glass, favouring
658 the alteration process leading to the browning phenomenon. Moreover, some studies correlate
659 the synthesis of siderophores to a subsequent oxidation of Mn to higher oxidation states (III,
660 IV), that are also commonly found in the characteristic brown phases of this pathology.
661 According to Duckworth and Sposito, 2005b, DFOB facilitates Mn^{2+} oxidation because it forms
662 strong complexes giving negative charge to the complexed Mn^{2+} , which lowers the activation
663 energy of the oxidation reaction and facilitates electron transfer from Mn(II) to O_2 . Parker et
664 al., 2007 showed that the wild strain *P. putida* produced the siderophore pyoverdine PVD that
665 formed a Mn(III) complex and then degraded to produce MnO_2 , thus showing that siderophore
666 production can be involved in the process of Mn oxides formation.
667 The Mn-siderophore affinity is so strong that it has been underlined by Peña et al., 2007 that
668 siderophore-promoted dissolution of Mn-minerals may compete with the siderophore-promoted
669 dissolution of Fe-minerals. Mn(III)-siderophore complexes may be present in natural
670 environments and may influence the speciation of manganese (Tebo et al., 2005; Duckworth et
671 al., 2009) as well as other natural compounds that can form Mn(III) complexes (sugar residuals
672 and microbially produced extracellular polysaccharides). Therefore, the study of Mn ligand-
673 promoted dissolution in silicate glass can also be of interest for the understanding of glass
674 alteration in other Mn-bearing natural and artificial glasses.

675

676 5. CONCLUSION

677 The dissolution kinetics of Mn-free and Mn-bearing medieval-like potash-lime-silicate glass
678 were investigated in aqueous solution in presence of biogenic exudates. The results show first
679 the role of MnO in the glass, that induces lower dissolution rates in control experiments, and
This article has been accepted for publication and undergone full peer review but has not been through
the copyediting, typesetting, pagination and proofreading process, which may lead to differences
between this version and the Version of Record. Please cite this article as:

<https://doi.org/10.1016/j.ibiod.2022.105442>

This article is protected by copyright. All rights reserved.

680 then the role of exudates. Oxalic acid enhances the dissolution rate as it favours interdiffusion
681 reactions and the complexation of Al and Mn from the glass. DFOB has a stronger effect on the
682 dissolution rates as it involves powerful ligand-promoted dissolution. In the two-ligands
683 system, no clear synergistic effect was observed. The results of this work show that a biological
684 activity could be involved in the solubilisation of Mn from a Mn-bearing glass, necessary step
685 of the appearance of the browning phenomenon. This work focused on the indirect impact that
686 microorganisms can have on the dissolution of this composition of glass. This step is necessary
687 in order to differentiate the indirect (via the production of metabolites) and the direct impact
688 (direct contact of microorganisms with glass). For better understanding of the role of
689 microorganisms on the appearance of this pathology, future work will focus on the direct impact
690 of microorganisms on Mn-bearing potash-lime-silicate glass alteration.

691

692 **ACKNOWLEDGMENTS**

693 This work was supported by the Paris Ile-de-France Region – DIM “Matériaux anciens et
694 patrimoniaux » and by the Doctoral school “Science Ingénierie et Environnement” of
695 Université Paris-Est. We thank Cyril Vaultot for the BET measurements and Nicolas Rividi for
696 assistance in microprobe analysis.

697

698 **RESEARCH DATA**

699 The research data, consisting of the raw results from the dissolution experiments are available
700 in the EarthChem Database [<https://doi.org/10.26022/IEDA/112217>].

701

702 **REFERENCES**

- 703 Ahmed E. and Holmström S. J. M. (2014) Siderophores in environmental research: Roles and
704 applications. *Microb. Biotechnol.* **7**, 196–208.
- 705 Akafia M. M., Harrington J. M., Bargar J. R. and Duckworth O. W. (2014) Metal
706 oxyhydroxide dissolution as promoted by structurally diverse siderophores and oxalate.
707 *Geochim. Cosmochim. Acta* **141**, 258–269.
- 708 Arletti R., Giacobbe C., Quartieri S., Sabatino G., Tigano G., Triscari M. and Vezzalini G.
709 (2010) Archaeometrical investigation of sicilian early byzantine glass: Chemical and
710 spectroscopic data. *Archaeometry* **52**, 99–114.

This article has been accepted for publication and undergone full peer review but has not been through the copyediting, typesetting, pagination and proofreading process, which may lead to differences between this version and the Version of Record. Please cite this article as:

<https://doi.org/10.1016/j.ibiod.2022.105442>

This article is protected by copyright. All rights reserved.

- 711 Asay D. B. and Kim S. H. (2005) Evolution of the adsorbed water layer structure on silicon
712 oxide at room temperature. *J. Phys. Chem. B* **109**, 16760–16763.
- 713 Bennett P. C., Melcer M. E., Siegel D. I. and Hassett J. P. (1988) The dissolution of quartz in
714 dilute aqueous solutions of organic acids at 25°C. *Geochim. Cosmochim. Acta* **52**, 1521–
715 1530.
- 716 Bernardi A., Becherini F., Bassato G. and Bellio M. (2006) Condensation on ancient stained
717 glass windows and efficiency of protective glazing systems: Two French case studies,
718 Sainte-Chapelle (Paris) and Saint-Urbain Basilica (Troyes). *J. Cult. Herit.* **7**, 71–78.
- 719 Bourleuf É. V. De, Ferrand J., Rossano S., Loisel C., Bauchau F., Bousta F., Oriol G.,
720 François A., Hullebusch E. Van, Trcera N. and Pallot-frossard I. (2011) Étude du
721 phénomène de brunissement de vitraux médiévaux The browning phenomenon of
722 medieval stained-glass windows. , 117–121.
- 723 Cagno S., Nuyts G., Bugani S., De Vis K., Schalm O., Caen J., Helfen L., Cotte M., Reischig
724 P. and Janssens K. (2011) Evaluation of manganese-bodies removal in historical stained
725 glass windows via SR- μ -XANES/XRF and SR- μ -CT. *J. Anal. At. Spectrom.* **26**, 2442–
726 2451.
- 727 Cailleteau C., Angeli F., Devreux F., Gin S., Jestin J., Jollivet P. and Spalla O. (2008a) Insight
728 into silicate-glass corrosion mechanisms. *Nat. Mater.* **7**, 978–983.
- 729 Cailleteau C., Weigel C., Ledieu A., Barboux P. and Devreux F. (2008b) On the effect of
730 glass composition in the dissolution of glasses by water. *J. Non. Cryst. Solids* **354**, 117–
731 123.
- 732 Calvaruso C., Turpault M. P., Frey-Klett P., Uroz S., Pierret M. C., Tosheva Z. and Kies A.
733 (2013) Increase of apatite dissolution rate by scots pine roots associated or not with
734 burkholderia glathei PML1(12)Rp in open-system flow microcosms. *Geochim.*
735 *Cosmochim. Acta* **106**, 287–306.
- 736 Cama J. and Ganor J. (2006) The effects of organic acids on the dissolution of silicate
737 minerals: A case study of oxalate catalysis of kaolinite dissolution. *Geochim.*
738 *Cosmochim. Acta* **70**, 2191–2209.
- 739 Carmona N., Laiz L., Gonzalez J. M., Garcia-Heras M. H., Villegas M. A. and Saiz-Jimenez
740 C. (2006) Biodeterioration of historic stained glasses from the Cartuja de Miraflores
741 (Spain). *Int. Biodeterior. Biodegrad.* **58**, 155–161.

This article has been accepted for publication and undergone full peer review but has not been through the copyediting, typesetting, pagination and proofreading process, which may lead to differences between this version and the Version of Record. Please cite this article as:

<https://doi.org/10.1016/j.ibiod.2022.105442>

This article is protected by copyright. All rights reserved.

- 742 Chalmin E., Farges F. and Brown G. E. (2009) A pre-edge analysis of Mn K-edge XANES
743 spectra to help determine the speciation of manganese in minerals and glasses. *Contrib.*
744 *to Mineral. Petrol.* **157**, 111–126.
- 745 Cheah S. F., Kraemer S. M., Cervini-Silva J. and Sposito G. (2003) Steady-state dissolution
746 kinetics of goethite in the presence of desferrioxamine B and oxalate ligands:
747 Implications for the microbial acquisition of iron. *Chem. Geol.* **198**, 63–75.
- 748 Drever J. I. and Stillings L. L. (1997) SURFACES The role of organic acids in mineral
749 weathering. *Colloids and Surfaces* **120**, 167–181.
- 750 Drewello R. and Weissmann R. (1997) Microbially influenced corrosion of glass. *Appl.*
751 *Microbiol. Biotechnol.* **47**, 337–346.
- 752 Duckworth O. W., Bargar J. R. and Sposito G. (2009) Coupled biogeochemical cycling of
753 iron and manganese as mediated by microbial siderophores. *BioMetals* **22**, 605–613.
- 754 Duckworth O. W. and Sposito G. (2005a) Siderophore-Manganese(III) interactions II.
755 Manganite dissolution promoted by desferrioxamine B. *Environ. Sci. Technol.* **39**, 6045–
756 6051.
- 757 Duckworth O. W. and Sposito G. (2005b) Siderophore-manganese (III) interactions. I. Air-
758 oxidation of manganese(II) promoted by desferrioxamine B. *Environ. Sci. Technol.* **39**,
759 6037–6044.
- 760 Faulkner K. M., Stevens R. D. and Fridovich I. (1994) Characterization of Mn(III) complexes
761 of linear and cyclic desferrioxamines as mimics of superoxide dismutase activity. *Arch.*
762 *Biochem. Biophys.* **310**, 341–346.
- 763 Fein J. B. and Hestrin J. E. (1994) Experimental studies of oxalate complexation at 80 °C:
764 Gibbsite, amorphous silica, and quartz solubilities in oxalate-bearing fluids. *Geochim.*
765 *Cosmochim. Acta* **58**, 4817–4829.
- 766 Ferrand J., Rossano S., Loisel C., Trcera N., Van Hullebusch E. D., Bousta F. and Pallot-
767 Frossard I. (2015) Browning Phenomenon of Medieval Stained Glass Windows. *Anal.*
768 *Chem.* **87**, 3662–3669.
- 769 Ferreira C. M. H., Pinto I. S. S., Soares E. V. and Soares H. M. V. M. (2015) (Un)suitability
770 of the use of pH buffers in biological, biochemical and environmental studies and their
771 interaction with metal ions-a review. *RSC Adv.* **5**, 30989–31003.
- 772 De Ferri L., Lottici P. P. and Vezzalini G. (2014) Characterization of alteration phases on

This article has been accepted for publication and undergone full peer review but has not been through the copyediting, typesetting, pagination and proofreading process, which may lead to differences between this version and the Version of Record. Please cite this article as:

<https://doi.org/10.1016/j.ibiod.2022.105442>

This article is protected by copyright. All rights reserved.

- 773 Potash-Lime-Silica glass. *Corros. Sci.* **80**, 434–441.
- 774 Fischer T. B., Heaney P. J. and Post J. E. (2018) Changes in the structure of birnessite during
775 siderophore-promoted dissolution: A time-resolved synchrotron X-ray diffraction study.
776 *Chem. Geol.* **476**, 46–58.
- 777 Fox T. R. and Comerford N. B. (1990) Low-Molecular-Weight Organic Acids in Selected
778 Forest Soils of the Southeastern USA. *Soil Sci. Soc. Am. J.* **54**, 1139–1144.
- 779 Furrer G. and Werner S. (1986) The coordination chemistry of weathering: dissolution
780 kinetics of δ -Al₂O₃ and BeO. *Geochim. Cosmochim. Acta* **50**, 1847–1860.
- 781 Gadd G. M. (1999) Fungal production of citric and oxalic acid: Importance in metal
782 speciation, physiology and biogeochemical processes. *Adv. Microb. Physiol.* **41**, 47–92.
- 783 Galois L., Calas G. and Arrio M. A. (2001) High-resolution XANES spectra of iron in
784 minerals and glasses: Structural information from the pre-edge region. *Chem. Geol.* **174**,
785 307–319.
- 786 Gentaz L., Lombardo T., Chabas A., Loisel C., Neff D. and Verney-Carron A. (2016) Role of
787 secondary phases in the scaling of stained glass windows exposed to rain. *Corros. Sci.*
788 **109**, 206–216.
- 789 Gentaz L., Lombardo T., Loisel C., Chabas A. and Vallotto M. (2011) Early stage of
790 weathering of medieval-like potash-lime model glass: Evaluation of key factors.
791 *Environ. Sci. Pollut. Res.* **18**, 291–300.
- 792 Gin S., Neill L., Fournier M., Frugier P., Ducasse T., Tribet M., Abdelouas A., Parruzot B.,
793 Neeway J. and Wall N. (2016) The controversial role of inter-diffusion in glass
794 alteration. *Chem. Geol.* **440**, 115–123.
- 795 Gislason S. R. and Oelkers E. H. (2003) Mechanism, rates, and consequences of basaltic glass
796 dissolution: II. An experimental study of the dissolution rates of basaltic glass as a
797 function of pH and temperature. *Geochim. Cosmochim. Acta* **67**, 3817–3832.
- 798 Gliozzo E. (2017) The composition of colourless glass: a review. *Archaeol. Anthropol. Sci.* **9**,
799 455–483.
- 800 Gorbushina A. A. and Palinska K. A. (1999) Biodeteriorative processes on glass:
801 experimental proof of the role of fungi and cyanobacteria. *Aerobiologia (Bologna)*. **15**,
802 183–191.
- 803 Gulmini M., Pace M., Ivaldi G., Ponzi M. N. and Mirti P. (2009) Morphological and chemical

This article has been accepted for publication and undergone full peer review but has not been through the copyediting, typesetting, pagination and proofreading process, which may lead to differences between this version and the Version of Record. Please cite this article as:

<https://doi.org/10.1016/j.ibiod.2022.105442>

This article is protected by copyright. All rights reserved.

- 804 characterization of weathering products on buried Sasanian glass from central Iraq. *J.*
805 *Non. Cryst. Solids* **355**, 1613–1621.
- 806 Hausrath E. M., Neaman A. and Brantley S. L. (2009) Elemental release rates from dissolving
807 basalt and granite with and without organic ligands. *Am. J. Sci.* **309**, 633–660.
- 808 Hernlem B. J., Vane L. M. and Sayles G. D. (1994) Stability constants of pseudobactin
809 complexes with transition metals. *Soil Sci. Soc. Am. J.* **58**, 390–396.
- 810 Hersman L., Lloyd T. and Sposito G. (1995) Siderophore-promoted dissolution of hematite.
811 *Geochim. Cosmochim. Acta* **59**, 3327–3330.
- 812 Holmén B. A. and Casey W. H. (1996) Hydroxamate ligands, surface chemistry, and the
813 mechanism of ligand-promoted dissolution of goethite [α -FeOOH(s)]. *Geochim.*
814 *Cosmochim. Acta* **60**, 4403–4416.
- 815 Huang W. H. and Keller W. D. (1972) © 1972 Nature Publishing Group. *Nat. new Biol.* **239**,
816 149–151.
- 817 Jackson C. M. (2005) Making colourless glass in the Roman period. *Archaeometry* **47**, 763–
818 780.
- 819 Jantzen C. M. and Plodinec M. (1984) Thermodynamic model of natural, medieval and
820 nuclear waste glass durability. *Glass* **67**, 207–223.
- 821 Jun Y. S. and Martin S. T. (2003) Microscopic observations of reductive manganite
822 dissolution under oxic conditions. *Environ. Sci. Technol.* **37**, 2363–2370.
- 823 Kalinowski B. E., Liermann L. J., Brantley S. L., Barnes A. and Pantano C. G. (2000) X-ray
824 photoelectron evidence for bacteria-enhanced dissolution of hornblende. *Geochim.*
825 *Cosmochim. Acta* **64**, 1331–1343.
- 826 Kendall T. A. and Hochella M. F. (2003) Measurement and interpretation of molecular-level
827 forces of interaction between the siderophore azotobactin and mineral surfaces.
828 *Geochim. Cosmochim. Acta* **67**, 3537–3546.
- 829 Kraemer S. M. (2004) Iron oxide dissolution and solubility in the presence of siderophores.
830 *Aquat. Sci.* **66**, 3–18.
- 831 Kraemer S. M., Cheah S. F., Zapf R., Xu J., Raymond K. N. and Sposito G. (1999) Effect of
832 hydroxamate siderophores on Fe release and Pb(II) adsorption by goethite. *Geochim.*
833 *Cosmochim. Acta* **63**, 3003–3008.
- 834 Kruff B. I., Harrington J. M., Duckworth O. W. and Jarzęcki A. A. (2013) Quantum

This article has been accepted for publication and undergone full peer review but has not been through the copyediting, typesetting, pagination and proofreading process, which may lead to differences between this version and the Version of Record. Please cite this article as:

<https://doi.org/10.1016/j.ibiod.2022.105442>

This article is protected by copyright. All rights reserved.

- 835 mechanical investigation of aqueous desferrioxamine B metal complexes: Trends in
836 structure, binding, and infrared spectroscopy. *J. Inorg. Biochem.* **129**, 150–161.
- 837 Lazo D. E., Dyer L. G. and Alorro R. D. (2017) Silicate, phosphate and carbonate mineral
838 dissolution behaviour in the presence of organic acids: A review. *Miner. Eng.* **100**, 115–
839 123.
- 840 Lenting C., Plümper O., Kilburn M., Guagliardo P., Klinkenberg M. and Geisler T. (2018)
841 Towards a unifying mechanistic model for silicate glass corrosion. *npj Mater. Degrad.* **2**.
- 842 Li X. D. and Schwartz F. W. (2004) DNAPL remediation with in situ chemical oxidation
843 using potassium permanganate. Part I. Mineralogy of Mn oxide and its dissolution in
844 organic acids. *J. Contam. Hydrol.* **68**, 39–53.
- 845 Li Z. bo, Lu X., Teng H. H., Chen Y., Zhao L., Ji J., Chen J. and Liu L. (2019) Specificity of
846 low molecular weight organic acids on the release of elements from lizardite during
847 fungal weathering. *Geochim. Cosmochim. Acta* **256**, 20–34.
- 848 Lombardo T., Gentaz L., Verney-Carron A., Chabas A., Loisel C., Neff D. and Leroy E.
849 (2013) Characterisation of complex alteration layers in medieval glasses. *Corros. Sci.* **72**,
850 10–19.
- 851 Luo Y., Tan W., Suib S. L., Qiu G. and Liu F. (2018) Dissolution and phase transformation
852 processes of hausmannite in acidic aqueous systems under anoxic conditions. *Chem.*
853 *Geol.* **487**, 54–62.
- 854 Marvasi M., Vedovato E., Balsamo C., Macherelli A., Dei L., Mastromei G. and Perito B.
855 Bacterial community analysis on the Mediaeval stained glass window “Natività” in the
856 Florence Cathedral. *J. Cult. Herit.* **10**, 124–133.
- 857 Melcher M. and Schreiner M. (2006) Leaching studies on naturally weathered potash-lime-
858 silica glasses. *J. Non. Cryst. Solids* **352**, 368–379.
- 859 Mirti P., Davit P. and Gulmini M. (2002) Colourants and opacifiers in seventh and eighth
860 century glass investigated by spectroscopic techniques. *Anal. Bioanal. Chem.* **372**, 221–
861 229.
- 862 Mysen B. and Richet P. (2005) *Silicate Glasses and Melts Properties and Structure*. 1st ed.
863 ed. D. in Geochemistry, Elsevier.
- 864 Neaman A., Chorover J. and Brantley S. L. (2005) Implications of the evolution of organic
865 acid moieties for basalt weathering over geological time. *Am. J. Sci.* **305**, 147–185.

This article has been accepted for publication and undergone full peer review but has not been through the copyediting, typesetting, pagination and proofreading process, which may lead to differences between this version and the Version of Record. Please cite this article as:

<https://doi.org/10.1016/j.ibiod.2022.105442>

This article is protected by copyright. All rights reserved.

- 866 Nelson C. and White W. B. (1980) Transition metal ions in silicate melts-I. Manganese in
867 sodium silicate melts. *Geochim. Cosmochim. Acta* **44**, 887–893.
- 868 Neubauer U., Nowack B., Furrer G. and Schulin R. (2000) Heavy metal sorption on clay
869 minerals affected by the siderophore desferrioxamine B. *Environ. Sci. Technol.* **34**,
870 2749–2755.
- 871 Nuyts G., Cagno S., Bugani S. and Janssens K. (2015) Micro-XANES study on Mn browning:
872 Use of quantitative valence state maps. *J. Anal. At. Spectrom.* **30**, 642–650.
- 873 Oelkers E. H. and Gislason S. R. (2003) Mechanism, rates, and consequences of basaltic glass
874 dissolution: II. An experimental study of the dissolution rates of basaltic glass as a
875 function of pH and temperature. *Geochim. Cosmochim. Acta* **67**, 3817–3832.
- 876 Oriol G., Warscheid T., Bousta F. and Loisel C. (2007) Incidence bactérienne dans les
877 phénomènes de brunissement des vitraux anciens TT - Microbial impact in the browning
878 of old stained glass windows. *Actual. Chim.*, 34–39.
- 879 Parker D. L., Morita T., Mozafarzadeh M. L., Verity R., McCarthy J. K. and Tebo B. M.
880 (2007) Inter-relationships of MnO₂ precipitation, siderophore-Mn(III) complex
881 formation, siderophore degradation, and iron limitation in Mn(II)-oxidizing bacterial
882 cultures. *Geochim. Cosmochim. Acta* **71**, 5672–5683.
- 883 Parker D. L., Sposito G. and Tebo B. M. (2004) Manganese(III) binding to a pyoverdine
884 siderophore produced by a manganese(II)-oxidizing bacterium. *Geochim. Cosmochim.*
885 *Acta* **68**, 4809–4820.
- 886 Peña J., Duckworth O. W., Bargar J. R. and Sposito G. (2007) Dissolution of hausmannite
887 (Mn₃O₄) in the presence of the trihydroxamate siderophore desferrioxamine B.
888 *Geochim. Cosmochim. Acta* **71**, 5661–5671.
- 889 Perez A., Daval D., Fournier M., Vital M., Delaye J. M. and Gin S. (2019) Comparing the
890 reactivity of glasses with their crystalline equivalents: The case study of plagioclase
891 feldspar. *Geochim. Cosmochim. Acta* **254**, 122–141.
- 892 Perez A., Rossano S., Trcera N., Huguenot D., Fourdrin C., Verney-Carron A., van
893 Hullebusch E. D. and Guyot F. (2016) Bioalteration of synthetic Fe(III)-, Fe(II)-bearing
894 basaltic glasses and Fe-free glass in the presence of the heterotrophic bacteria strain
895 *Pseudomonas aeruginosa*: Impact of siderophores. *Geochim. Cosmochim. Acta* **188**, 147–
896 162.

This article has been accepted for publication and undergone full peer review but has not been through the copyediting, typesetting, pagination and proofreading process, which may lead to differences between this version and the Version of Record. Please cite this article as:

<https://doi.org/10.1016/j.ibiod.2022.105442>

This article is protected by copyright. All rights reserved.

- 897 Perez A., Rossano S., Trcera N., Verney-Carron A., Huguenot D., van Hullebusch E. D.,
898 Catillon G., Razafitianamaharavo A. and Guyot F. (2015) Impact of iron chelators on
899 short-term dissolution of basaltic glass. *Geochim. Cosmochim. Acta* **162**, 83–98.
- 900 Perezy Jorba M., Dallas J. P., Bauer C., Bahezre C. and Martin J. C. (1980) Deterioration of
901 stained glass by atmospheric corrosion and micro-organisms. *J. Mater. Sci.* **15**, 1640–
902 1647.
- 903 Piñar G., Garcia-Valles M., Gimeno-Torrente D., Fernandez-Turiel J. L., Ettenauer J. and
904 Sterflinger K. (2013) Microscopic, chemical, and molecular-biological investigation of
905 the decayed medieval stained window glasses of two Catalan churches. *Int.*
906 *Biodeterior. Biodegrad.* **84**, 388–400.
- 907 Poulson S. R., Drever J. I. and Stillings L. L. (1997) Aqueous Si-oxalate complexing, oxalate
908 adsorption onto quartz, and the effect of oxalate upon quartz dissolution rates. *Chem.*
909 *Geol.* **140**, 1–7.
- 910 Quartieri S., Triscari M., Sabatino G., Boscherini F. and Sani A. (2002) Fe and Mn K-edge
911 XANES study of ancient Roman glasses. *Eur. J. Mineral.* **14**, 749–756.
- 912 Reichard P. U., Kraemer S. M., Frazier S. W. and Kretzschmar R. (2005) Goethite dissolution
913 in the presence of phytosiderophores: Rates, mechanisms, and the synergistic effect of
914 oxalate. *Plant Soil* **276**, 115–132.
- 915 Renshaw J. C., Robson G. D., Trinci A. P. J., Wiebe M. G., Livens F. R., Collison D. and
916 Taylor R. J. (2002) Fungal siderophores: Structures, functions and applications. *Mycol.*
917 *Res.* **106**, 1123–1142.
- 918 Rodrigues A., Gutierrez-Patricio S., Miller A. Z., Saiz-Jimenez C., Wiley R., Nunes D.,
919 Vilarigues M. and Macedo M. F. (2014) Fungal biodeterioration of stained-glass
920 windows. *Int. Biodeterior. Biodegrad.* **90**, 152–160.
- 921 Rölleke S., Gurtner C., Drewello U., Drewello R., Lubitz W. and Weissmann R. (1999)
922 Analysis of bacterial communities on historical glass by denaturing gradient gel
923 electrophoresis of PCR-amplified gene fragments coding for 16S rRNA. *J. Microbiol.*
924 *Methods* **36**, 107–114.
- 925 Saal L. B. and Duckworth O. W. (2010) Synergistic Dissolution of Manganese Oxides as
926 Promoted by Siderophores and Small Organic Acids. *Soil Sci. Soc. Am. J.* **74**, 2021–
927 2031.

This article has been accepted for publication and undergone full peer review but has not been through the copyediting, typesetting, pagination and proofreading process, which may lead to differences between this version and the Version of Record. Please cite this article as:

<https://doi.org/10.1016/j.ibiod.2022.105442>

This article is protected by copyright. All rights reserved.

- 928 Salek S. S., Kleerebezem R., Jonkers H. M., Voncken J. H. L. and Van Loosdrecht M. C. M.
929 (2013) Determining the impacts of fermentative bacteria on wollastonite dissolution
930 kinetics. *Appl. Microbiol. Biotechnol.* **97**, 2743–2752.
- 931 Schabereiter-Gurtner C., Piñar G., Lubitz W. and Rölleke S. (2001) Analysis of fungal
932 communities on historical church window glass by denaturing gradient gel
933 electrophoresis and phylogenetic 18S rDNA sequence analysis. *J. Microbiol. Methods*
934 **47**, 345–354.
- 935 Schalm O., Proost K., De Vis K., Cagno S., Janssens K., Mees F., Jacobs P. and Caen J.
936 (2011) Manganese staining of archaeological glass: The characterization of mn-rich
937 inclusions in leached layers and a hypothesis of its formation. *Archaeometry* **53**, 103–
938 122.
- 939 Schijf J., Christenson E. A. and Potter K. J. (2015) Different binding modes of Cu and Pb vs.
940 Cd, Ni, and Zn with the trihydroxamate siderophore desferrioxamine B at seawater ionic
941 strength. *Mar. Chem.* **173**, 40–51.
- 942 Sessegolo L., Verney-Carron A., Ausset P., Nowak S., Triquet S., Saheb M. and Chabas A.
943 (2020) Alteration rate of medieval potash-lime silicate glass as a function of pH and
944 temperature: A low pH-dependent dissolution. *Chem. Geol.* **550**, 119704.
- 945 Sessegolo L., Verney-Carron A., Saheb M., Remusat L., Gonzalez-Cano A., Loisel C. and
946 Chabas A. (2017) Water Transport within Ancient Stained Glass Alteration Layer using
947 Oxygen Isotopes. *Procedia Earth Planet. Sci.* **17**, 814–817.
- 948 Sessegolo L., Verney-Carron A., Saheb M., Remusat L., Gonzalez-Cano A., Nuns N., Mertz
949 J.-D., Loisel C. and Chabas A. (2018) Long-term weathering rate of stained-glass
950 windows using H and O isotopes. *npj Mater. Degrad.* **2**, 17.
- 951 Staudigel H. and Hart S. R. (1983) Alteration of basaltic glass: Mechanisms and significance
952 for the oceanic crust-seawater budget. *Geochim. Cosmochim. Acta* **47**, 337–350.
- 953 Sterpenich J. and Libourel G. (2001) Using stained glass windows to understand the durability
954 of toxic waste matrices. *Chem. Geol.* **174**, 181–193.
- 955 Tang Y., Zeiner C. A., Santelli C. M. and Hansel C. M. (2013) Fungal oxidative dissolution
956 of the Mn(II)-bearing mineral rhodochrosite and the role of metabolites in manganese
957 oxide formation. *Environ. Microbiol.* **15**, 1063–1077.
- 958 Tebo B. M., Johnson H. A., McCarthy J. K. and Templeton A. S. (2005) Geomicrobiology of

This article has been accepted for publication and undergone full peer review but has not been through the copyediting, typesetting, pagination and proofreading process, which may lead to differences between this version and the Version of Record. Please cite this article as:

<https://doi.org/10.1016/j.ibiod.2022.105442>

This article is protected by copyright. All rights reserved.

- 959 manganese(II) oxidation. *Trends Microbiol.* **13**, 421–428.
- 960 Thorseth I. H., Pedersen R. B. and Christie D. M. (2003) Microbial alteration of 0-30-Ma
961 seafloor and sub-seafloor basaltic glasses from the Australian Antarctic Discordance.
962 *Earth Planet. Sci. Lett.* **215**, 237–247.
- 963 Torres M. A., Dong S., Nealson K. H. and West A. J. (2019) The kinetics of siderophore-
964 mediated olivine dissolution. *Geobiology* **17**, 401–416.
- 965 Tournié A., Majérus O., Lefèvre G., Rager M. N., Walmé S., Caurant D. and Barboux P.
966 (2013) Impact of boron complexation by Tris buffer on the initial dissolution rate of
967 borosilicate glasses. *J. Colloid Interface Sci.* **400**, 161–167.
- 968 Tournié A., Ricciardi P. and Colomban P. (2008) Glass corrosion mechanisms: A multiscale
969 analysis. *Solid State Ionics* **179**, 2142–2154.
- 970 Trcera N., Rossano S. and Tarrida M. (2011) Structural study of Mg-bearing sodosilicate
971 glasses by Raman spectroscopy. *J. Raman Spectrosc.* **42**, 765–772.
- 972 Verney-Carron A., Sessegolo L., Saheb M., Valle N., Ausset P., Losno R., Mangin D.,
973 Lombardo T., Chabas A. and Loisel C. (2017) Understanding the mechanisms of Si-K-
974 Ca glass alteration using silicon isotopes. **203**, 404–421.
- 975 Wang Y. and Stone A. T. (2006) Reaction of Mn^{III,IV} (hydr)oxides with oxalic acid,
976 glyoxylic acid, phosphonoformic acid, and structurally-related organic compounds.
977 *Geochim. Cosmochim. Acta* **70**, 4477–4490.
- 978 Weaver J. L., DePriest P. T., Plymale A. E., Pearce C. I., Arey B. and Koestler R. J. (2021)
979 Microbial interactions with silicate glasses. *npj Mater. Degrad.* **5**, 1–18.
- 980 Welch S. A. and Ullman W. J. (1993) The effect of organic acids on plagioclase dissolution
981 rates and stoichiometry. *Geochim. Cosmochim. Acta* **57**, 2725–2736.
- 982 Woisetschläger G., Dutz M., Paul S. and Schreiner M. (2000) Weathering phenomena on
983 naturally weathered potash-lime-silica-glass with medieval composition studied by
984 secondary electron microscopy and energy dispersive microanalysis. *Mikrochim. Acta*
985 **135**, 121–130.
- 986 Wolff-Boenisch D., Gislason S. R., Oelkers E. H. and Putnis C. V. (2004) The dissolution
987 rates of natural glasses as a function of their composition at pH 4 and 10.6, and
988 temperatures from 25 to 74°C. *Geochim. Cosmochim. Acta* **68**, 4843–4858.
- 989 Wolff-Boenisch D. and Traina S. J. (2006) A comparative study of the effect of

This article has been accepted for publication and undergone full peer review but has not been through the copyediting, typesetting, pagination and proofreading process, which may lead to differences between this version and the Version of Record. Please cite this article as:

<https://doi.org/10.1016/j.ibiod.2022.105442>

This article is protected by copyright. All rights reserved.

990 desferrioxamine B, oxalic acid, and Na-alginate on the desorption of U(VI) from goethite
991 at pH 6 and 25 °C. *Geochim. Cosmochim. Acta* **70**, 4356–4366.

992 Wolff-Boenisch D. and Traina S. J. (2007) The effect of desferrioxamine B, enterobactin,
993 oxalic acid, and Na-alginate on the dissolution of uranyl-treated goethite at pH 6 and
994 25 °C. *Chem. Geol.* **243**, 357–368.

995
996
997
998
999
1000

1001
1002
1003
1004
1005
1006
1007
1008
1009
1010
1011
1012
1013
1014
1015
1016
1017
1018
1019
1020
1021
1022
1023
1024

This article has been accepted for publication and undergone full peer review but has not been through the copyediting, typesetting, pagination and proofreading process, which may lead to differences between this version and the Version of Record. Please cite this article as:

<https://doi.org/10.1016/j.ibiod.2022.105442>

This article is protected by copyright. All rights reserved.

1025 Table 1 Composition (in oxide weight %) obtained by microprobe analysis – when available -
 1026 of the three synthesized glasses. Standard deviations are calculated on 10 measures performed
 1027 on each sample.

Wt %	Mn-bearing glass (VM)	Mn-free glass (VNM)	½ Mn-bearing glass (VM1/2)
SiO ₂	51.5 ± 0.4	52.4 ± 0.5	51.3
Al ₂ O ₃	1.8 ± 0.0	1.9 ± 0.1	2.0
P ₂ O ₅	3.2 ± 0.2	3.4 ± 0.3	3.8
Na ₂ O	1.2 ± 0.0	1.2 ± 0.0	1.4
CaO	17.3 ± 0.2	17.6 ± 0.2	17.4
MgO	4.3 ± 0.1	4.3 ± 0.1	4.4
K ₂ O	18.3 ± 0.1	18.8 ± 0.3	19.0
MnO	2.0 ± 0.1	0.0 ± 0.1	1.0
Total	99.8 ± 0.3	99.7 ± 0.4	100

1028
 1029
 1030
 1031
 1032
 1033
 1034
 1035
 1036
 1037
 1038
 1039

This article has been accepted for publication and undergone full peer review but has not been through the copyediting, typesetting, pagination and proofreading process, which may lead to differences between this version and the Version of Record. Please cite this article as:

<https://doi.org/10.1016/j.ibiod.2022.105442>

This article is protected by copyright. All rights reserved.

1040 Table 2 Si initial dissolution rates r_{Si} ($\text{g m}^{-2} \text{d}^{-1}$) and final (after 3 days of experiment) average
 1041 pH for all experimental condition. Uncertainties for dissolution rates correspond to the absolute
 1042 error calculated taking into account the analytical ICP-OES error (10%), the uncertainty on the
 1043 reactive surface area (8%), and - when the experiment was repeated - the experimental error
 1044 \pm SD for the experimental replicates. Uncertainties for pH correspond to the standard deviation
 1045 of the replicates measurements. The starting pH is 6.8 ± 0.1 .

	VM		VM1/2		VNM	
	r_{Si}	pH	r_{Si}	pH	r_{Si}	pH
[C]	0.40 ± 0.08	8.5 ± 0.3	0.50	8.7	0.80 ± 0.14	9.1 ± 0.3
[DFOB 50 μM]	0.83 ± 0.11	8.8 ± 0.5				
[DFOB 100 μM]	0.99 ± 0.16	8.8 ± 0.5				
[DFOB 250 μM]	1.20 ± 0.21	8.9 ± 0.0				
[DFOB 500 μM]	1.43 ± 0.23	8.7 ± 0.1			1.32 ± 0.24	8.7 ± 0.1
[DFOB 1000 μM]	1.50 ± 0.20	8.3 ± 0.1				
[OA 1 mM]	0.64 ± 0.09	8.9 ± 0.1			1.13 ± 0.15	9.3 ± 0.1
[OA 1 mM DFOB 50 μM]	0.89 ± 0.16	9.1 ± 0.1				
[OA 1 mM DFOB 100 μM]	1.15 ± 0.15	9.3 ± 0.0				
[OA 1 mM DFOB 250 μM]	1.62 ± 0.27	9.2 ± 0.1				
[OA 1 mM DFOB 500 μM]	1.38 ± 0.20	8.8 ± 0.0				

1046

1047

This article has been accepted for publication and undergone full peer review but has not been through the copyediting, typesetting, pagination and proofreading process, which may lead to differences between this version and the Version of Record. Please cite this article as:

<https://doi.org/10.1016/j.ibiod.2022.105442>

This article is protected by copyright. All rights reserved.

1048 List of figures

1049

1050 Figure 1. Schematic draw of the experimental design for all the dissolution conditions tested.

1051

1052 Figure 2. Average normalized mass losses versus time for the three control experiments: a)
1053 VNM glass, b) VM1/2 glass c) VM glass. Error bars correspond to the uncertainties calculated
1054 taking into account the analytical ICP-OES error (10%), and - when the experiment was
1055 repeated - the standard deviation for the replicates.

1056

1057 Figure 3. Average normalized mass losses versus time for the experiments for VNM and VM
1058 glass with exudates: a) VNM glass in OA 1 mM, b) VM glass in OA 1 mM , c) VNM glass in
1059 DFOB 500 μM , d) VM glass in DFOB 500 μM , e) VM glass OA 1mM + DFOB 500 μM . Error
1060 bars correspond to the uncertainties calculated taking into account the analytical ICP-OES error
1061 (10%), and the standard deviation for the replicates.

1062 Figure 4. (a) Mn average normalised mass losses versus time for the experiments of VM glass
1063 in different DFOB concentrations. Error bars correspond to the uncertainties calculated taking
1064 into account the analytical ICP-OES error (10%) and the standard deviation for the replicates.
1065 (b) UV- VIS absorbance of the Mn(III)HDFOB⁺ complex measured at 310 nm for the
1066 dissolution tests of VM glass in different DFOB concentrations. Error bars correspond to the
1067 standard deviation for the two experimental replicates.

1068 Figure 5. Si initial dissolution rates ($\text{g m}^2 \text{d}^{-1}$) calculated for the studied glasses for the control
1069 conditions. Error bars correspond to the absolute error calculated taking into account the
1070 analytical ICP-OES error (10%), the uncertainty on the reactive surface area (8%), and the
1071 standard deviation for the replicates.

1072 Figure 6. Si dissolution rate values ($\text{g m}^2 \text{d}^{-1}$) plotted as a function of DFOB concentration (μM)
1073 for the DFOB one-ligand system and for the two-ligand system with [OA 1 mM + DFOB]. The
1074 threshold effect is visible by the inflection of the curve and stagnation of dissolution rates values
1075 starting from [DFOB 250 μM] for both the one and two-ligands systems. Error bars correspond
1076 to the uncertainties calculated taking into account the analytical ICP-OES error (10%) and the
1077 standard deviation for the two experimental replicates.

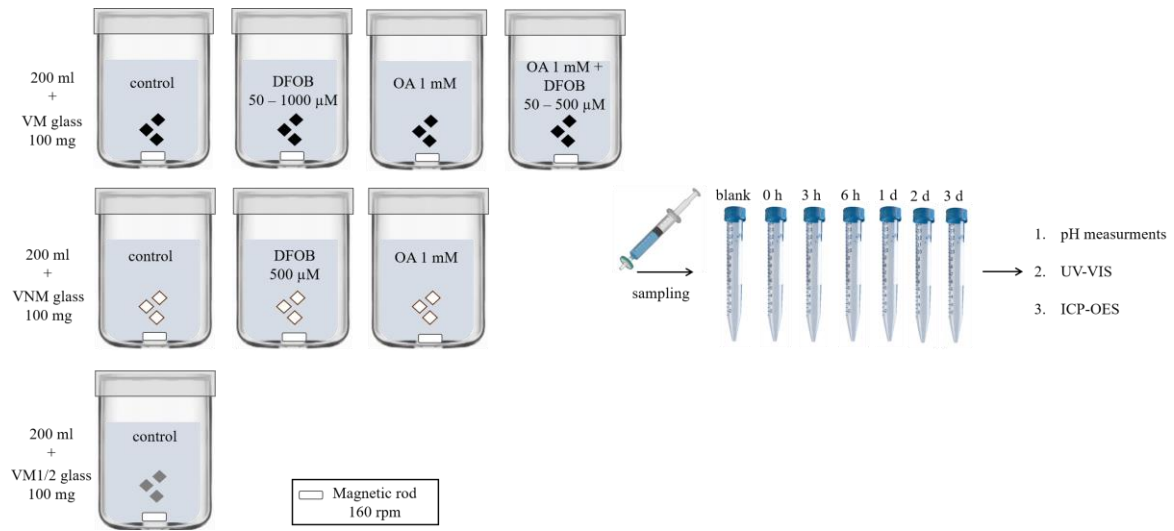
This article has been accepted for publication and undergone full peer review but has not been through
the copyediting, typesetting, pagination and proofreading process, which may lead to differences
between this version and the Version of Record. Please cite this article as:

<https://doi.org/10.1016/j.ibiod.2022.105442>

This article is protected by copyright. All rights reserved.

1078
1079
1080
1081
1082

Figure 1



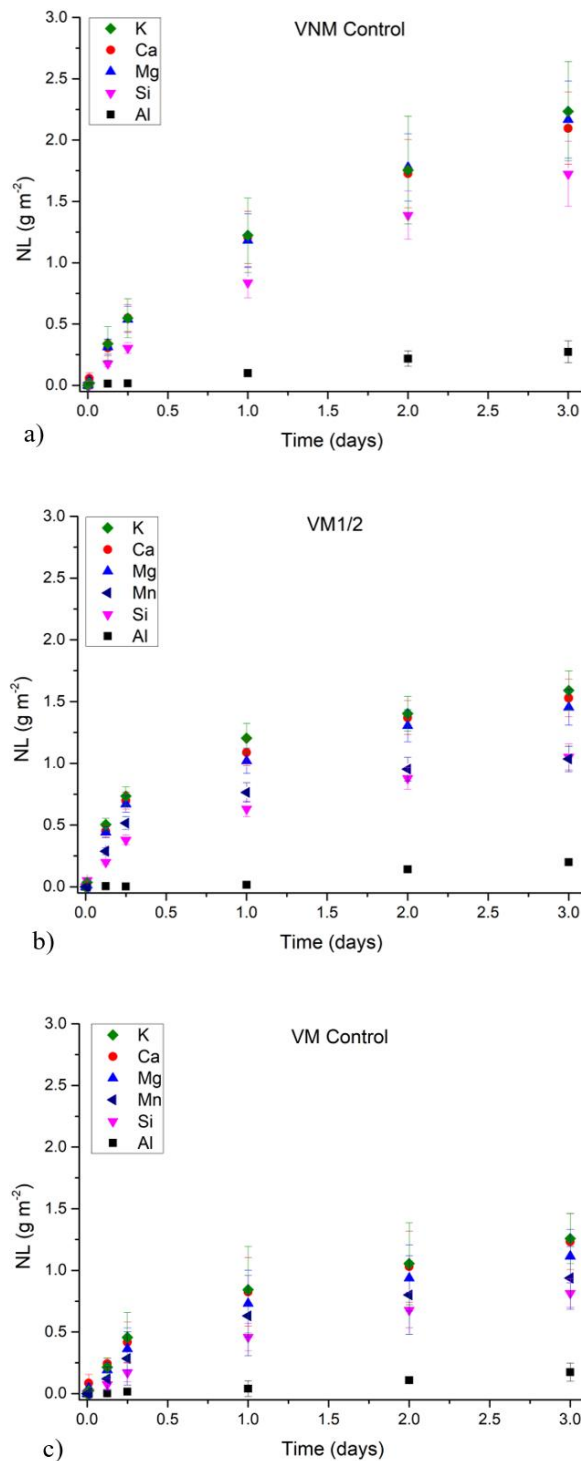
1083
1084
1085
1086
1087
1088
1089
1090
1091
1092
1093
1094
1095
1096
1097
1098
1099
1100
1101
1102
1103
1104
1105
1106
1107
1108
1109
1110

This article has been accepted for publication and undergone full peer review but has not been through the copyediting, typesetting, pagination and proofreading process, which may lead to differences between this version and the Version of Record. Please cite this article as:

<https://doi.org/10.1016/j.ibiod.2022.105442>

This article is protected by copyright. All rights reserved.

1111 Figure 2
1112

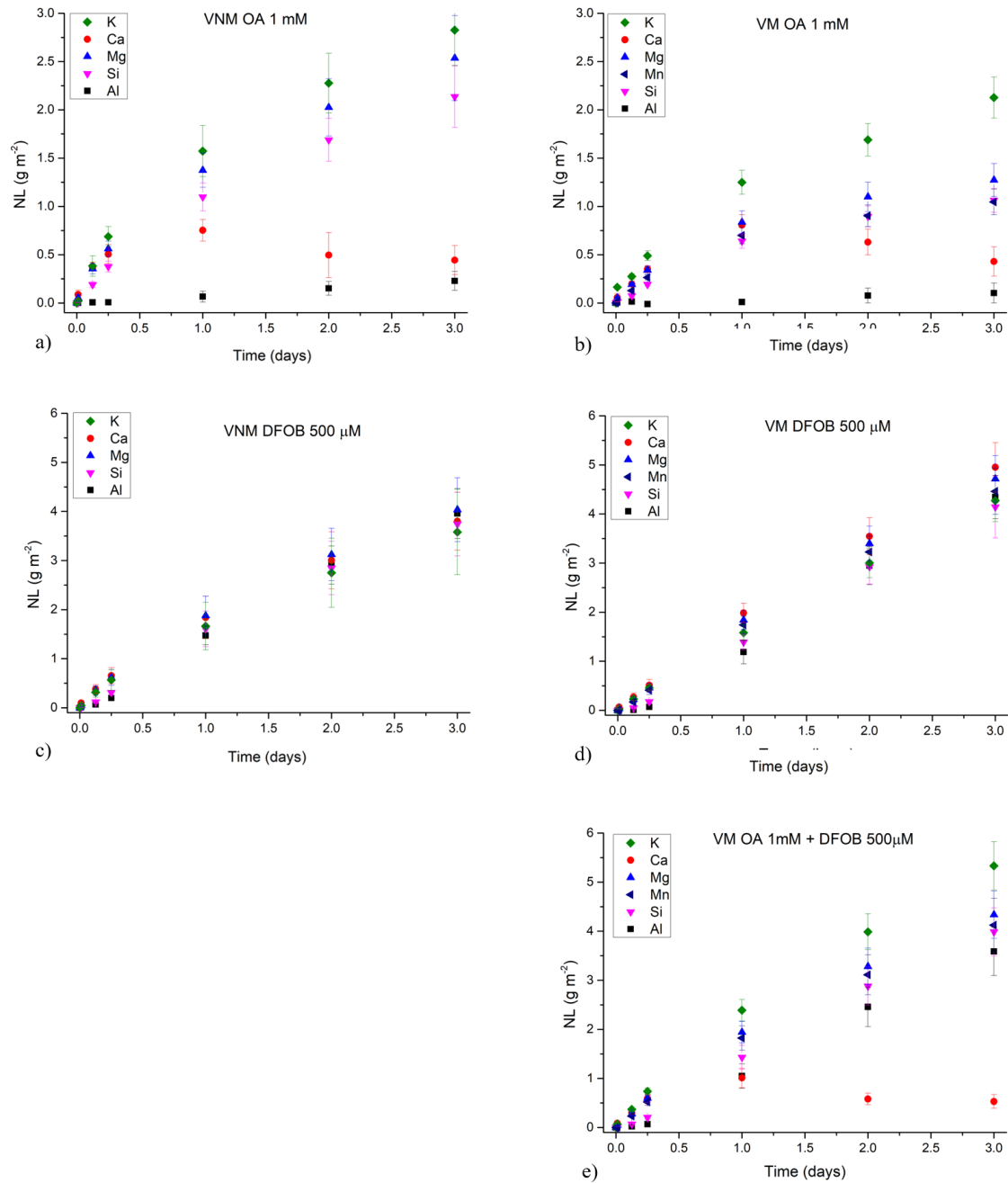


1113
1114

This article has been accepted for publication and undergone full peer review but has not been through the copyediting, typesetting, pagination and proofreading process, which may lead to differences between this version and the Version of Record. Please cite this article as:

<https://doi.org/10.1016/j.ibiod.2022.105442>

This article is protected by copyright. All rights reserved.



1116

1117

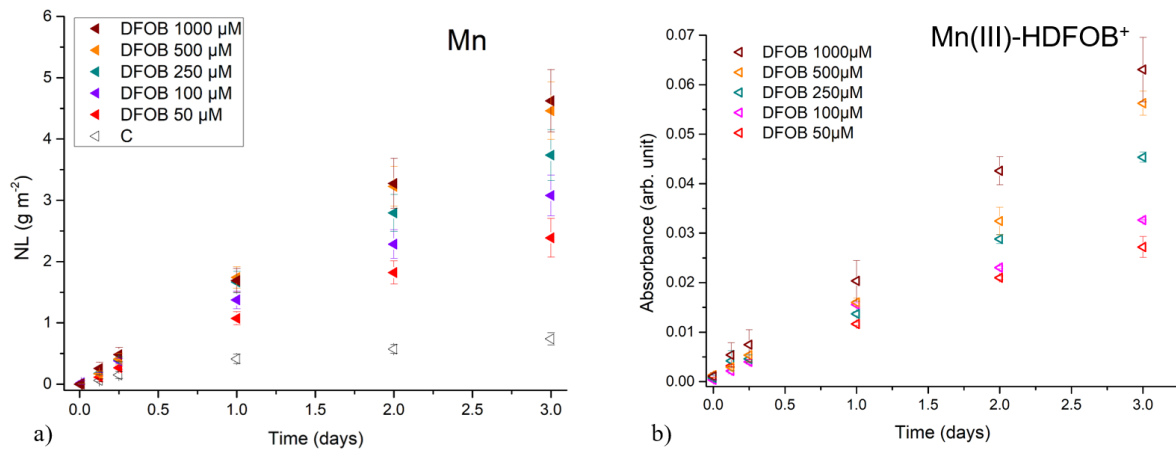
1118

This article has been accepted for publication and undergone full peer review but has not been through the copyediting, typesetting, pagination and proofreading process, which may lead to differences between this version and the Version of Record. Please cite this article as:

<https://doi.org/10.1016/j.ibiod.2022.105442>

This article is protected by copyright. All rights reserved.

1119 **Figure 4**



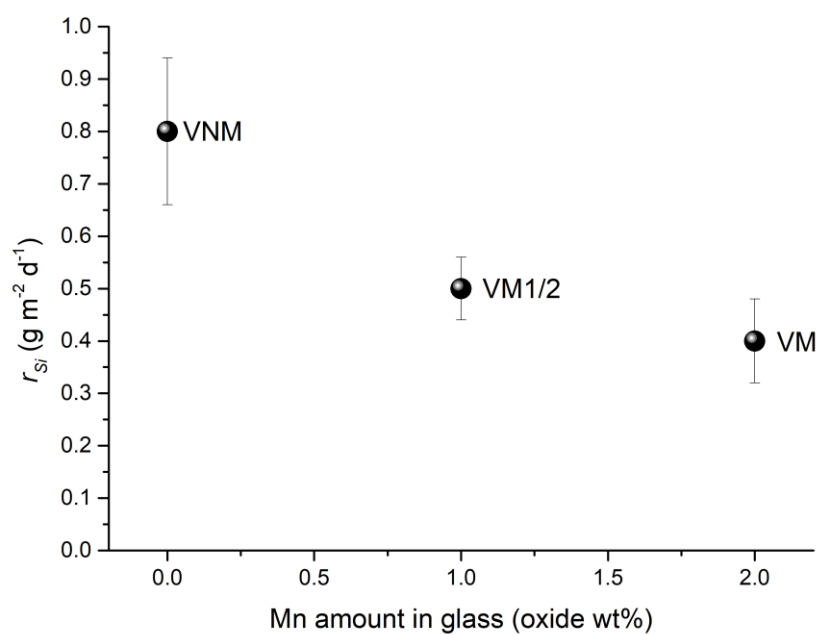
1120

1121

This article has been accepted for publication and undergone full peer review but has not been through the copyediting, typesetting, pagination and proofreading process, which may lead to differences between this version and the Version of Record. Please cite this article as:

<https://doi.org/10.1016/j.ibiod.2022.105442>

This article is protected by copyright. All rights reserved.



1123

1124

1125

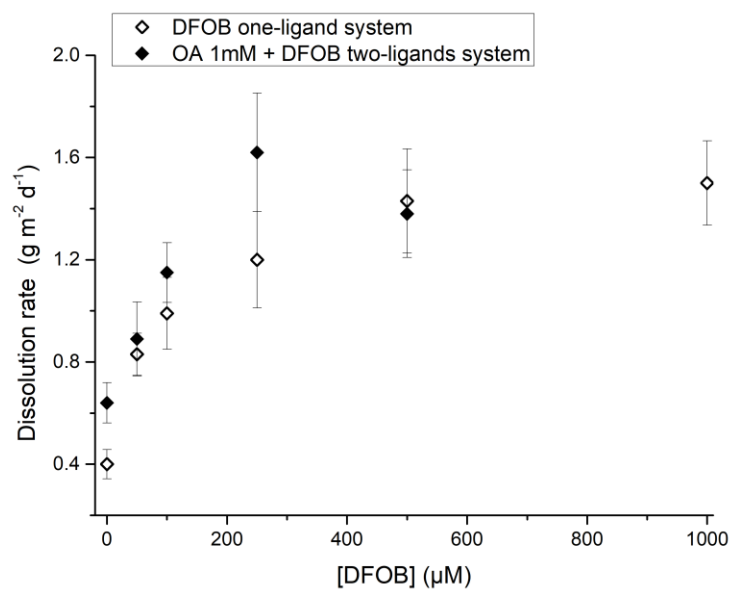
This article has been accepted for publication and undergone full peer review but has not been through the copyediting, typesetting, pagination and proofreading process, which may lead to differences between this version and the Version of Record. Please cite this article as:

<https://doi.org/10.1016/j.ibiod.2022.105442>

This article is protected by copyright. All rights reserved.

1126 Figure 6

1127



1128

1129

This article has been accepted for publication and undergone full peer review but has not been through the copyediting, typesetting, pagination and proofreading process, which may lead to differences between this version and the Version of Record. Please cite this article as:

<https://doi.org/10.1016/j.ibiod.2022.105442>

This article is protected by copyright. All rights reserved.